APPLIED SCIENCES AND ENGINEERING

ECM-inspired micro/nanofibers for modulating cell function and tissue generation

Yun Xu[1,2]*, Guodong Shi[2]*, Jincheng Tang[1]*, Ruoyu Cheng[3], Xiaofeng Shen[4], Yong Gu[1], Liang Wu[1], Kun Xi[1], Yihong Zhao[2], Wenguo Cui[1,3]†, Liang Chen[1]†

Current homogeneous bioscaffolds could hardly recapture the regenerative microenvironment of extracellular matrix. Inspired by the peculiar nature of dura matter, we developed an extracellular matrix–mimicking scaffold with biomimetic heterogeneous features so as to fit the multiple needs in dura mater repairing. The inner surface endowed with anisotropic topology and optimized chemical cues could orchestrate the elongation and bipolarization of fibroblasts and preserve the quiescent phenotype of fibroblasts indicated by down-regulated α–smooth muscle actin expression. The outer surface could suppress the fibrotic activity of myofibroblasts via increased microfiber density. Furthermore, integrin β1 and Yes-associated protein molecule signaling activities triggered by topological and chemical cues were verified, providing evidence for a potential mechanism. The capability of the scaffold in simultaneously promoting dura regeneration and inhibiting epidural fibrosis was further verified in a rabbit laminectomy model. Hence, the so-produced heterogeneous fibrous scaffold could reproduce the microstructure and function of natural dura.

INTRODUCTION

Characterized by high complexity and inhomogeneity, the microstructure of extracellular matrix (ECM) has been extensively studied in multiple tissue types such as bone, fibrocartilage, Achilles tendon, and ligament. Despite the great diversity among different tissues, the architecture and composition of ECM always play pivotal roles in the maintenance of physiological homeostasis and the progression of pathological conditions (*1*). Because of an incomprehensive understanding of the relationships between ECM microstructure and tissue function, the current design of scaffolds with homogeneous architecture for connective tissue regeneration could hardly reproduce the highly complex and heterogeneous structure of ECM so as to achieve structural regeneration and functional recovery (*2*). Therefore, there is an urgent need to fabricate a heterogeneous ECM-inspired tissue-engineered platform resembling the microstructures, physicochemical properties of natural ECM to promote the recovery of tissue morphology and function. ECM inspired us to design biomimetic nanofibers to determine what effects ECM network imposes on multiple cell events.

As the connective tissue membrane surrounding the spinal cord, dura mater has a complex microstructure and multiple physiological functions and tends to be subject to damages during practice of spinal surgery and results in epidural fibrosis, which could bring a series of complications. Dura mater contains collagenous fibers, which are arranged in parallel along the longitude direction with a few disorderedly distributed ones intertwining with each other, forming a multilayer heterogeneous network and showing distinct functionalities on different sides (*3*). In the context of dura mater damage, fibroblasts play intricate roles in both dura regeneration and fibrosis formation and put forward a difficult task for traditional homogeneous scaffolds in modulating cellular activities. The goal of repairing damaged dura tissue not only lies in promoting natural healing of dura mater through promoting fibroblast activity but also asks for effective prevention of arachnoiditis and neurological deficit caused by fibrosis, which is derived from excessive ECM component (collagen and fibronectin) deposition in the laminectomy area due to persistently activated and proliferated myofibroblasts. Enlighted by the microstructure and functionality of dura mater and the formation mechanism of tissue fibrosis, we thought that homogeneous scaffolds could be further tailored for better reproduction of the heterogeneous microstructure and endowed with the capability to regulate different cell activity so as to fit the need for dura mater repair.

Biomimetic biomaterials such as hydrogel three-dimensional (3D) scaffolds (*4*), micro/nanogrooved substrate (*5*), self-assembly protein networks (*6*), and electrospun fibrous membranes (*7*) are characterized by hierarchical microstructure similar with ECM, which could modulate multiple cell behaviors. Among diverse techniques constructing ECM-like microstructure, electrospinning has been widely used because of its facile procedure and versatile capability. Controllable parameters during electrospinning also allowed for the preparation of hierarchical and heterogeneous microstructure and superior reproduction of specific ECM network (*8*). Recent studies have suggested the complex roles of topological cues, fiber density, chemical composition, and other physicochemical properties of electrospun fibers on modulating cellular adhesion, proliferation, migration, phenotype, and differentiation. For instance, controlling the topographical architecture and pore size of electrospun scaffold could modulate the adhesion state and morphology of fibroblasts (*9*). A beneficial effect of an anisotropic electrospun matrix has been revealed during its application in promoting healing and suppressing scar tissue formation, which could be potentially attributed to the down-regulated α–smooth muscle actin (α-SMA) expression and inhibited differentiation of fibroblasts into

[1]Department of Orthopedics, The First Affiliated Hospital of Soochow University, Orthopedic Institute, Soochow University, 708 Renmin Road, Suzhou, Jiangsu 215006, P.R. China. [2]Departments of Pain Rehabilitation and Orthopaedic Surgery, Shanghai Public Health Clinical Center, Fudan University, 2901 Caolang Road, Shanghai 201500, P.R. China. [3]Shanghai Key Laboratory for Prevention and Treatment of Bone and Joint Diseases, Shanghai Institute of Traumatology and Orthopaedics, Ruijin Hospital, Shanghai Jiao Tong University School of Medicine, 197 Ruijin Second Road, Shanghai 200025, P.R. China. [4]Department of Orthopaedic Surgery, Suzhou TCM Hospital Affiliated to Nanjing University of Chinese Medicine, 889 Wuzhong West Road, Suzhou, Jiangsu 215006, P.R. China.
*These authors contributed equally to this work.
†Corresponding author. Email: wgcui80@hotmail.com (W.C.); chenliang1972@sina.com (L.C.)

contractile myofibroblasts (*10*, *11*). However, the particular mechanism of the effect of anisotropic topographical structure on maintaining fibroblast phenotype remains elusive. It has been suggested that the phenotypic transition could be associated with alteration on cell elongation and cytoskeleton organization and tension. Integrin β1 has been extensively studied on its key role in fibroblast mechanotransduction signaling and tissue fibrosis (*12*). Martin *et al.* (*13*) reported that the differentiation of fibroblasts into myofibroblasts involved the activation of transcription coactivator YAP (Yes-associated protein), a key mediator of integrin β1 signaling, which has been demonstrated to be regulated by cell morphology and stress fibers (*14*). To this end, it is reasonable to hypothesize that cell morphology and stress fibers of cytoskeleton regulated by topological cues and that chemical composition of electrospun fibers may participate in the activation of fibroblast into myofibroblast.

In this study, inspired by the heterogeneous microstructure of dura matter, a dual-layer heterogeneous micro/nanofiber structure was fabricated with an inner anisotropic layer maintaining the quiescent fibroblast phenotype and an outer dense layer inhibiting myofibroblast adhesion so as to simultaneously mimic the dual functions of dura matter in promoting tissue healing and preventing tissue fibrosis. In vitro modulation of the heterogeneous fiber scaffold on cellular behaviors of fibroblast/myofibroblast including adhesion morphology, proliferation, and phenotypic differentiation were thoroughly characterized to investigate the effect of fiber density, topology, and chemistry cues. Further exploration on intracellular biomarker activities was also conducted to reveal the mechanism potentially involved in the repair of dura matter and suppression of fibrosis. In addition, the physiochemical property of the heterogeneous fiber scaffold was characterized to ensure the capability of scaffolds to maintain stability in epidural space. Last but not the least, the effect of the dual-layer heterogeneous fiber scaffold was further verified in vivo by applying the scaffold in a rabbit laminectomy model and accessing its effectiveness on promoting healing and suppressing epidural fibrosis (Fig. 1).

RESULTS

Fabricated micro/nanofibers with tunable fiber alignment and composition

The micro/nanofiber-electrospun fibers with different collecting times (30, 60, 120, and 240 s, and 1 and 2 hours), various type I collagen (COL-I) blending ratios [mass ratio of COL-I to silk (SF): 5:95, 10:90, 15:85, 20:80, 25:75, and 50:50%), and distinct surface topology (random or anisotropic) were prepared with other parameters well controlled. The surface morphology of the fibers was observed via scanning electron microscopy (SEM) (Fig. 2, A and B), which showed a smooth surface structure on all scaffold fibers. The aligned SF/COL-I fibers (ASCF) were arranged in a regular and parallel direction, while the random SF/COL-I fibers (RSCF) were arranged in disorder and interwoven into a network. The fiber structure of random SF fibers (RSF) scaffolds was similar to that of RSCF, but the fiber density increases and the fiber aperture decreases along with the increase of collecting time (Fig. 2C). The diameter of RSF remained to be 824 ± 98 nm with different collecting time. Yet, upon the increase of collagen proportion, the diameter of blended fibers gradually decreased. No substantial difference was found between the diameter of anisotropic and random electrospun SF/COL fibers. The diameter of the 95:5% SF-COL fiber was found to be 804 ± 77 nm, while SF-COL–blended fiber diameters of 90:10, 85:15, 80:20, 75:25, and 50:50% were 618 ± 89, 487 ± 70, 454 ± 81, 433 ± 63, and 337 ± 65 nm, respectively. It has been reported that the diameter of a polyurethane composite fiber blended with gelatin decreased because of the reduced viscosity upon the addition of gelatin (*15*). Similarly, the diameter of the SF/COL-I–blended fiber decreased with the increase of collagen concentration, as has been evidenced in other literature (*16*), which attributed the diameter decrease to the reduced viscosity after collagen incorporation. When the concentration ratio of SF/COL-I reached 50:50%, frequent occurrence of fiber breakage could be found in the random composite nanofibers (Fig. 2B). However, fiber fracture was barely observed in the orientated nanofibers. The possible reason for such phenomenon could be that the mechanical properties of the electrospun membranes were compromised because of the increase of the collagen proportion, and different degrees of mechanical stress were loaded from all directions on the random fibers, causing more fiber fractures. The chemical composition of ASCF was characterized using Fourier transform infrared (FTIR) spectroscopy (fig. S1, A and B), which indicated increasing peak intensity along with increasing COL-I ratio in fibers and verified the successful blending of SF and COL-I in fibers.

Microstructure and chemical cues of fibrous substrates modulated multiple cellular behaviors

Characteristic of keloid fibroblasts

Fibroblasts from human skin and keloid tissue were cultured on cell culture dish and grew in good condition after passage. After adhesion to dish, no obvious difference in cell morphology was observed between the two types of cells. The cells were spreading in a flat shape, with elliptical nuclei. F-actin cytoskeleton staining showed that human skin keloid fibroblasts had higher cytoskeleton tension, compared with human skin fibroblasts, indicated by obvious stress fibers formed in keloid fibroblasts (fig. S2). The fluorescent staining of focal adhesion (FA) protein vinculin showed that keloid fibroblasts formed a large number of punctate- and needle-like sticky spots on the edges and in the cytoplasm, indicating significantly greater FA formation compared with human fibroblasts (fig. S2, A and B). The staining of α-SMA showed that the α-SMA expression in fibroblasts was limited to the cytoplasm, without obvious stress fiber formation, indicating the cell phenotype of fibroblasts. On the other hand, keloid fibroblasts expressed obvious α-SMA in the cytoplasm, which was integrated with the stress fibers, confirming keloid fibroblast as α-SMA–activated phenotype (fig. S2, C and D).

Integrin β1 activation

Integrin, as one of the mediators of cellular adhesion to ECM, plays an important role in regulating cell behavior. To verify the effect of the nanotopology and chemical composition of the electrospun fiber on the activation of integrin, the fibroblasts were seeded in the nanofiber matrix with different topological structures and chemical composition, and after culturing for 12 hours, immunofluorescence staining and flow cytometry were used to detect the activation of integrin β1. As shown in Fig. 3A, the distribution of integrin β1 was in accordance with actin cytoskeleton and identified at the plasma membrane. The fibroblast presented a well-spreading shape in random SF/COL fibers (RSCF) with highly expressed integrin β1. Elongated cell morphology was observed in anisotropic fibers (ASCF), accompanied by a significantly lower expression of integrin β1. As shown in Fig. 3 (B to F), the results of flow cytometry revealed that with the increase of collagen concentration in nanofibers, the

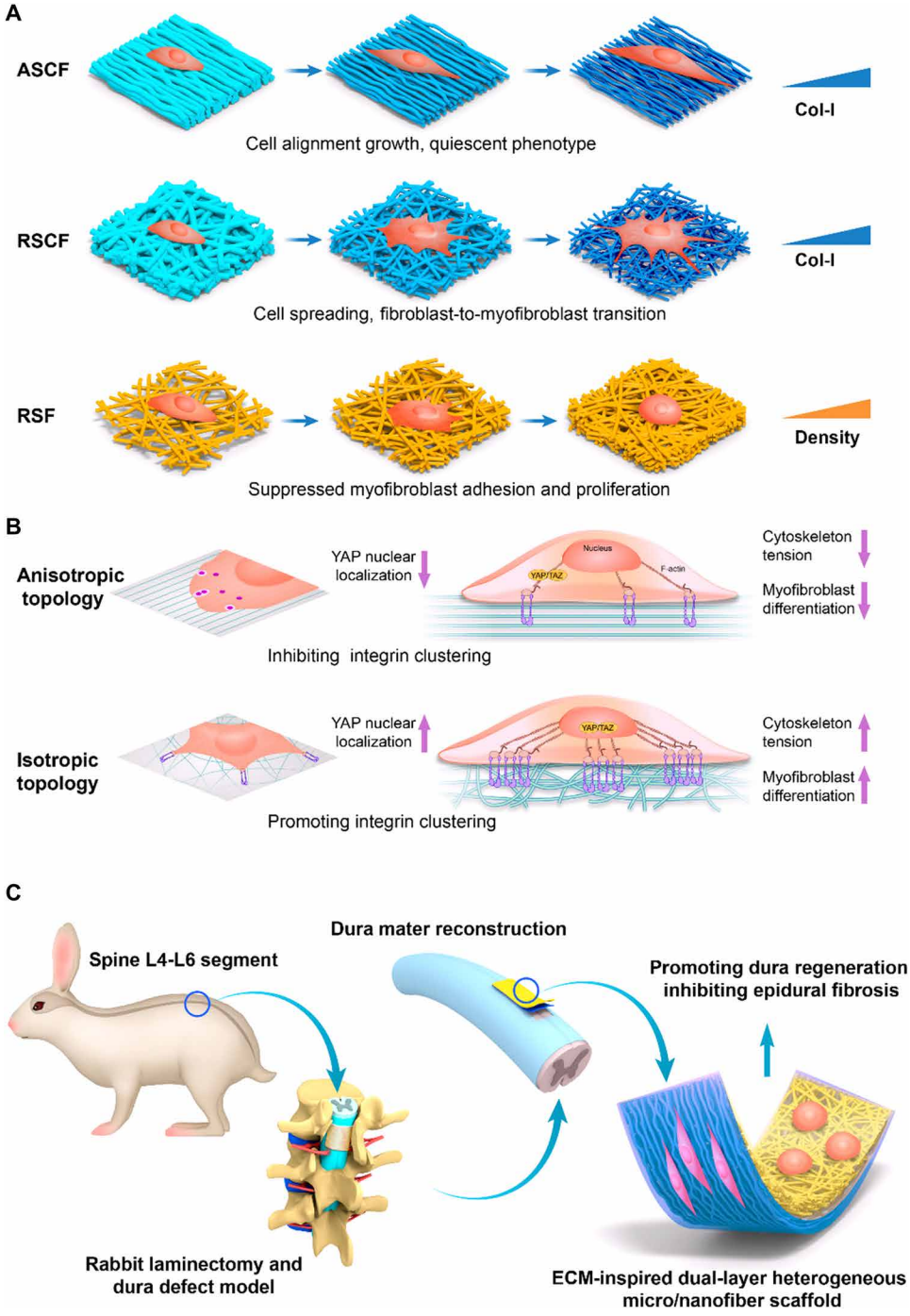

Fig. 1. Schematic illustration of heterogeneous micro/nanofibers modulating multiple cell behaviors to repair dura defect and prevent epidural fibrosis. (**A**) Electrospun micro/nanofibers modulate cell adhesion, proliferation and differentiation by topographic microstructure, chemical cues, and fiber density. ASCF, aligned SF/COL-I fibers; RSCF, random SF/COL-I fibers; RSF, random SF fibers. (**B**) Mechanism of anisotropic topographical structure on suppressing fibroblasts to myfibroblast transition by inhibiting integrin clustering, reorganizing cytoskeleton and reducing cell tension, and inhibiting YAP nuclear localization. (**C**) Schematic illustration of surgical procedure for creating dura defect in rabbits and implantation of biomimetic designed scaffolds for promoting the regeneration of dura mater and preventing epidural fibrosis.

ratio of activated integrin β1 on the fibroblasts cultured in both anisotropic and random electrospun nanofibers increased to varying degrees. However, under the same COL-I blending ratio, the integrin activation ratio of cells cultured on random nanofibers was significantly higher than that of the anisotropic fiber matrix. The cells cultured in the random nanofiber matrix of 50:50% SF/COL-I blend were found with an activation ratio of 69.53 ± 2.70%, compared with 51.23 ± 1.71% on the anisotropic electrospun fiber matrix, showing significant difference ($P < 0.001$) (Fig. 3F). This result indicated that the increase of COL-I concentration raises the adhesion

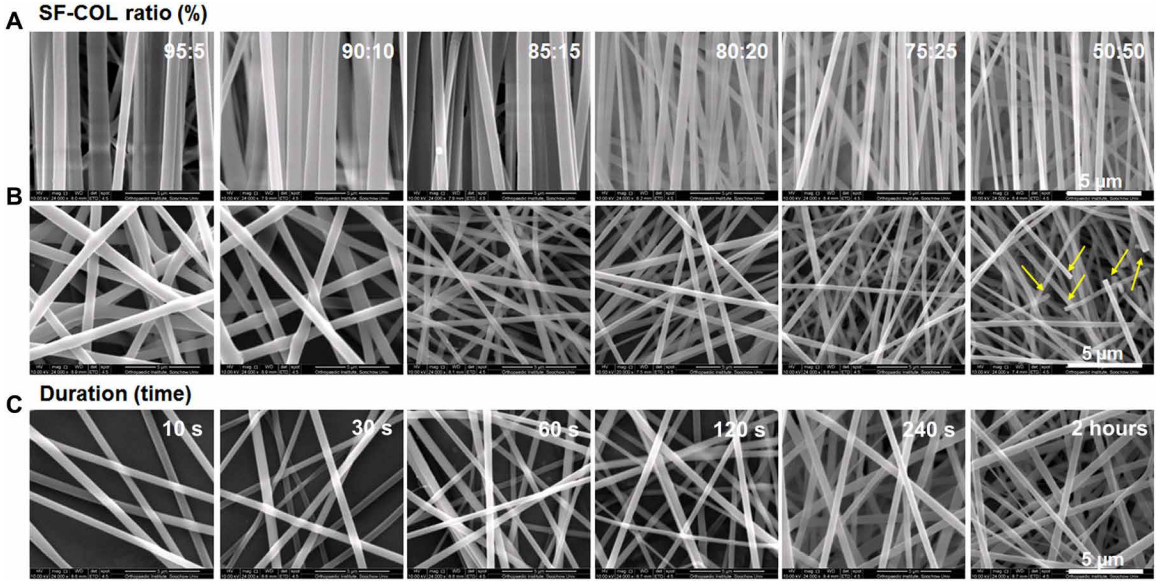

Fig. 2. Characterization of electrospun fibers. (**A** to **C**) SEM images of (A) ASCF and (B) RSCF containing gradient COL-I ratio and (C) SF fibers with varying densities (yellow arrow indicating fiber fracture).

ligand density, which promoted higher integrin β1 activation level. The topological microstructure of the fiber matrix could change the integrin activation state of the adhesion-binding interface between the cells and the matrix. Our results demonstrated that anisotropic topology significantly suppressed the activation of integrin β1. Previous studies have shown that the stiffness and topology of the matrix can change the level of integrin activation and expression. Under the same matrix stiffness, the surface topology of the patterned nanoscale microgrooves can reduce the expression level of integrin (*17*). Similar trends could be detected in our study as those previously reported, which could be attributed to the anisotropic electrospun surface topology similar to a nanogroove structure.

FA reorganization

To investigate the influence of the anisotropic topology and chemical composition of the electrospun fibers on the morphology and FA formation of fibroblasts, the expression of vinculin was characterized by immunofluorescence staining. As shown in Fig. 3, vinculin was expressed in the cytoplasm of in fibroblasts seeded in both random and anisotropic SF/COL-I fiber matrices. On the random SF/COL-I blend nanofibers, as cells adhered to the matrix, vinculin was recruited to the FA complex, which was mainly expressed in the terminal fibrous bundles of the filopodia and the lamellipodia at the edge of the cell, showing a denser, punctate-shaped red fluorescence. With the increase of collagen density in the random fibers, the area of cell adhesion on nanofibers increased significantly, as well as the expression of vinculin, indicated by fluorescence enhancement and enlarged quantity of punctate sticky spots at the ends of the filaments of the spreading cells (Fig. 3G, b, and fig. S4). In contrast, the red punctate-shaped signal of vinculin was almost absent in anisotropic fibers with the low collagen blending ratio groups (5, 10, and 15%). Only a slight increase on adhesion area and the fluorescent signal could be identified upon the increase of collagen ratio to 25 and 50% in anisotropic groups (Fig. 3G, a, and fig. S3). The above results indicated that the anisotropic topological structure of electrospun fibers can significantly change the adhesion state of cells in the matrix.

The effect of fiber density on FA was also investigated. As shown in Fig. 3G (c) and fig. S5, myofibroblasts cultured on SF-electrospun scaffolds with lower fiber density (30, 60, and 120 s) mainly expressed vinculin in the cytoplasm without obvious punctate FA formation. The expression of vinculin decreases if there is increase in fiber density. In the high-density nanofiber substrates, the myofibroblast F-actin becomes spherical, and the morphology of vinculin also shrank within the globular cytoplasm. In comparison, the myofibroblasts cultured in the tissue culture–treated polystyrene (TCPS) plates of the control group were completely spread out, with dense punctate sticky spots that appeared at the end of lamellipodia and filopodia (Fig. 3G, TCPS, and fig. S5, TCPS), indicating the significant effect of higher fiber density on inhibiting FA formation.

Cell morphology, spreading, and proliferation

After 48 hours of culturing on different fibers, the cells were stained with cytoskeleton and observed under both a fluorescent microscope (fig. S6) and a SEM (Fig. 4). The fibroblasts cultured on the alignment SF/COL-I substrates displayed a spindle shape and obvious elongation and bipolarization and grown along with the long axis of the anisotropic electrospun fibers because of the contact guidance of topology (Fig. 4A and fig. S6A). On the other hand, the cells on random fibers spread out in different directions and formed large lamellipodia. In addition, cell morphology was also affected by the increase of COL-I ratio in fibers. When the ratio of collagen increased from 25 to 50%, the cells on both random and anisotropic fibers exhibited significantly increased spreading area and higher cell density indicated by frequent cell fusion (Fig. 4B and fig. S6B). These results showed that upon the increase of the adhesion ligand density on the electrospun matrix, the interaction between cells and the matrix could be enhanced, with the adhesion and spreading of the cell also significantly improved, which was consistent with previous reports.

Because of the strong contractile phenotype possessed by myofibroblasts, tissue fibrosis and even pathological contracture could be elicited in the later period of wound healing under the continuous activation state of myofibroblasts (*18*). The contractile force of a

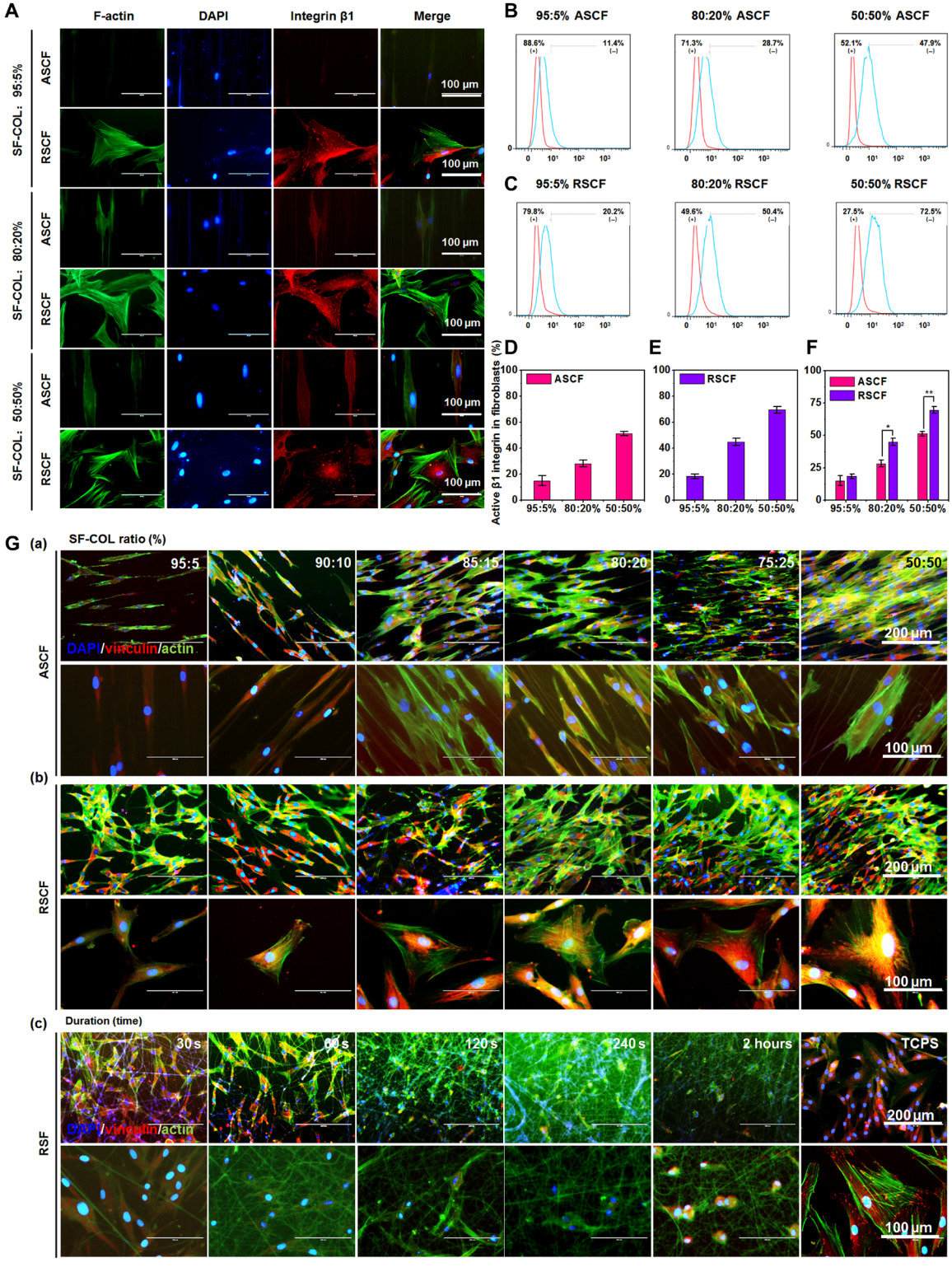

Fig. 3. Heterogeneous micro/nanofibers could affect the expression of integrin β1 and vinculin. (**A**) Immunofluorescence staining of integrin β1 in fibroblasts cultured on ASCF and RSDF containing varying COL-I content (5, 20, and 50%). DAPI, 4′,6-diamidino-2-phenylindole. (**B** and **C**) Flow cytometry of fibroblasts cultured on ASCF and RSCF containing varying COL-I content (5, 20, and 50%). (**D**) Integrin β1 activation rate of fibroblasts on ASCF. (**E**) Integrin β1 activation rate of fibroblasts on RSCF. (**F**) Comparison on integrin β1 activation rate of fibroblasts on ASCF and RSCF under various COL-I ratios (5, 20, and 50%). Statistically significant differences were indicated by $^{*}P < 0.05$ and $^{**}P < 0.01$ when comparing between ASCF and RSCF groups. (**G**) Immunofluorescence staining of vinculin in cells cultured on different fibers. (a and b) Immunofluorescence staining of vinculin in fibroblasts cultured on (a) ASCF and (b) RSCF containing gradient COL-I ratios, heterogeneous microstructure, and chemical cues. (c) Immunofluorescence staining of vinculin in myofibroblasts cultured on RSF with different fiber densities.

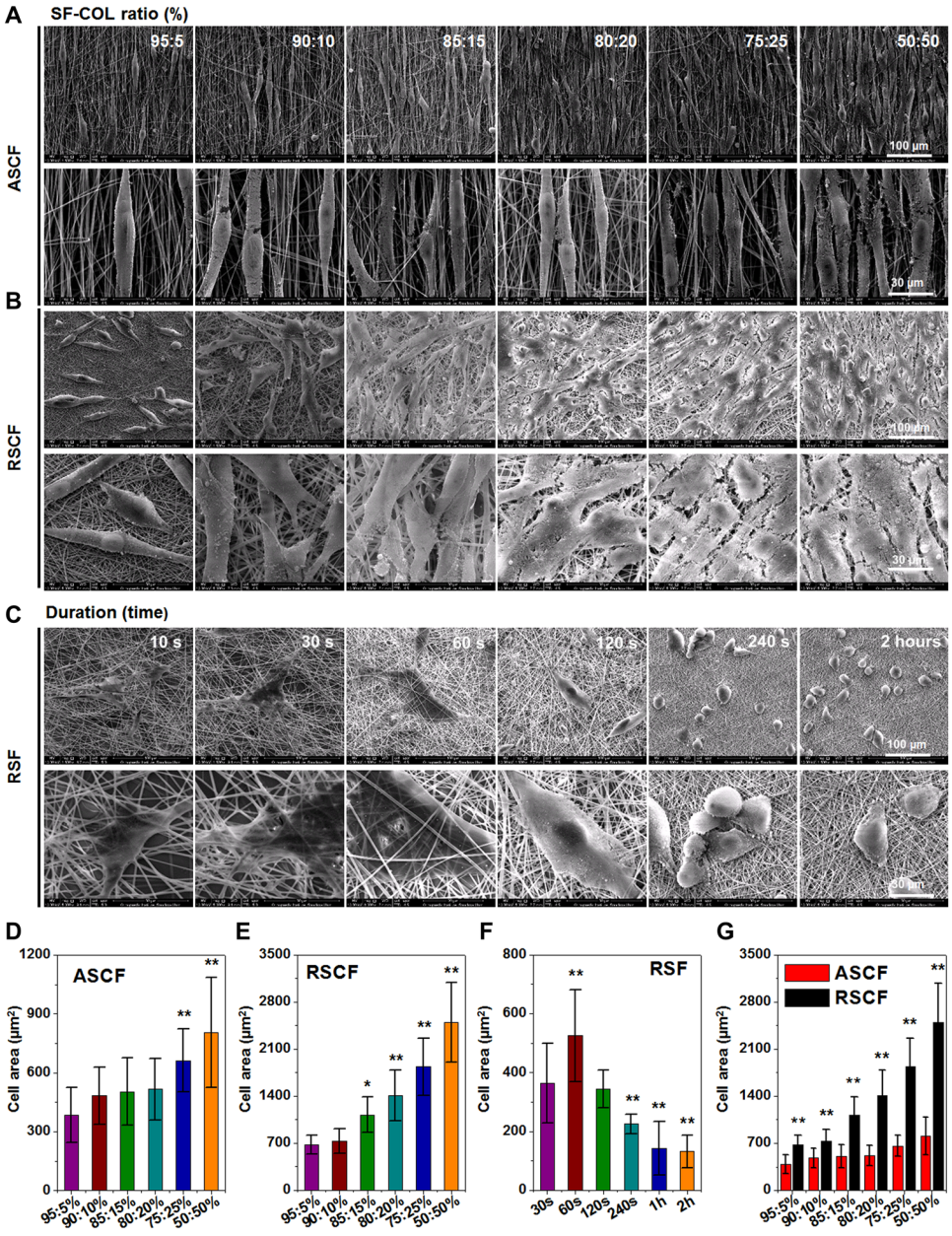

Fig. 4. SEM characterization of fibroblasts and myofibroblasts cultured on different fibers after culturing for 3 days. (**A** and **B**) Morphology of fibroblasts cultured on (A) ASCF and (B) RSCF containing gradient COL-I ratios. (**C**) Morphology of myofibroblasts cultured on RSF with different fiber densities. (**D** and **E**) Quantification of cell spreading area of fibroblasts cultured on (D) ASCF and (E) RSCF containing gradient COL-I ratios. (**F**) Cell spreading area of myofibroblasts cultured on RSF with different fiber densities. (**G**) Comparison of fibroblast spreading area on ASCF and RSCF under the same COL-I content. Statistically significant differences were indicated by $^{*}P < 0.05$ and $^{**}P < 0.01$ when comparing between ASCF and RSCF groups. (D and E) Statistically significant differences were indicated by $^{*}P < 0.05$ and $^{**}P < 0.01$ when comparing with the 30-s group (F); statistically significant differences were indicated by $^{**}P < 0.01$ when comparing between ASCF and RSCF groups (G).

myofibroblast could lead to membrane scaffold deformation when it was implanted in vivo. The loss of microstructure caused by scaffold deformation could aggravate hypertrophic scar contraction (*19*). Therefore, we prepared SF-electrospun fibers with different density to observe the interaction between myofibroblast and SF-electrospun fiber, as well as the adhesion, morphology, and spreading state of the cells on the different density fiber scaffolds in hopes of finding an optimized parameter for the suppression of myofibroblast contraction. Indicated by results of F-actin staining (fig. S6C) and SEM (Fig. 4C), myofibroblasts on the SF fibers with smaller density (collecting time of less than 120 s) spread into an irregular and polygonal shape. SEM images shown that myofibroblasts entangled with adjacent electrospun fibers, which were clearly recruited and deformed (Fig. 4C,10 and 30 s). However, upon the increase of fiber density, the amount of adhered cells on SF fibers significant decreased and the morphology of myofibroblasts shrunk obviously. Myofibroblast could hardly spread out while exhibited spherical morphology (Fig. 4C, 240 s and 2 hours). In addition, deformation of fibers surrounding

cells was rarely observed compared with fibers with lower density. These results indicated that an increasing density of SF-electrospun fiber could have a significant suppressing effect on the adhesion and spreading of myofibroblasts, and the compact structure from SF fibers with higher density could significantly inhibit the contractile force of myofibroblasts.

As one of the indicators of cell-material interaction, the spreading area of fibroblasts and myofibroblasts seeded on different fibers was investigated on the basis of SEM images. With the increase of the COL-I blending ratio in the electrospun fiber, the spreading area of the fibroblasts on both ASCF and RSCF fibrous matrices increased in varying degrees (Fig. 4, D and E). Under the same COL-I ratio, anisotropic topology of ASCF matrix was found to significantly reduce the spreading area compared with RSCF (Fig. 4G). As for the myofibroblasts seeded on RSF fibers, the corresponding spreading area was significantly down-regulated by increasing fiber density (Fig. 4F). These results indicated that both the chemical properties and topological microstructure of the substrate can produce significant effects on the spreading of the cells.

Integrin-ECM binding promotes cell adhesion to matrix, promotes the formation of FA, and activates the FA kinase (FAK), which would be further responsible for the mediation of multiple cell signaling pathways associated with the cellular proliferation, such as RhoA stimulation for contraction of myosin and acceleration of proliferation (*20*), and Cdc4/Rac1 stimulation for the formation of lamellipodia and pseudopodia (*21*). Cell viability determined by cell counting kit-8 (CCK-8) assay, as indicated by CCK-8 results (fig. S6, D and E), the proliferation rate of fibroblasts on the anisotropic or random SF/COL fiber matrix with a different composition ratio, was revealed to increase with prolonging of culturing time. At the same time point, especially at 3 and 5 days, the increase of collagen ratio resulted in the significant elevation of proliferation rate on both anisotropic and random fiber substrates, indicating the beneficial biological effect of COL-I composition. However, under the same COL-I ratio and time point, the proliferation rate of cells cultured on anisotropic fibers was significantly lower than that of random fibers (fig. S6G), revealing that a random fiber matrix could significantly promote cell adhesion and proliferation. The main reason for such difference is that, relative to anisotropic fibers that presented compact structure, random fibers had loosen structure, larger pores, and higher density of cell-adhesive ligands, all of which coordinately contributed to the promoting effect on proliferation. Previously, endothelial progenitor cells have been found to respond to the micro/nanogroove structure on which the cell elongated and aligned along the groove structure, exhibiting lower proliferation rate yet accelerated migration (*22*). In the current study, according to the differences on proliferation rate, together with SEM views (Fig. 4, A and B), distinct cell morphology and proliferating condition could be identified between random and anisotropic fibers with one later showing significantly elongated morphology and a smaller spreading area. This revealed the contact guidance effect from anisotropic topology on cellular morphology and on the proliferation activity of cells.

Extracted from silkworm cocoons, regenerated silk fibroin has been applied widely in tissue engineering as a biomaterial. Previous studies have shown that the SF protein matrix has good biocompatibility and supports the adhesion and proliferation of multiple cell types, such as fibroblasts, osteoblasts, skin keratinocytes, mesenchymal stem cells, and chondrocytes (*23*). However, few studies have investigated the effect of the density of SF-electrospun fiber scaffolds on cell behavior. We chose myofibroblasts with a high contractile phenotype to be cultured onto the SF-electrospun fiber scaffold. An upward trend could be observed in all groups with the time prolonging. On day 3 after culture, significant difference could be found on the proliferation rate of cells on different fibers with a higher density group (collecting time of 2 hours), exhibiting a significantly lower proliferation rate. Such difference became more significant on day 5, as reflected by a significantly lower proliferation rate on fibers with collecting time of 240 s and 1 and 2 hours (fig. S6F). These results indicated that the density of electrospun fibers could affect cell proliferation.

Phenotypic differentiation and ECM reorganization of fibroblasts

During the process of tissue healing, the quiescent fibroblasts are activated, characterized by the formation of α-SMA stress fibers integrated with the cytoskeleton F-actin. Activated fibroblasts with strong contractile force are responsible for enhanced secretion of ECM, which could facilitate wound contraction and tissue regeneration. However, persistent activation of fibroblasts could also enhance cell proliferation followed by the overproduction of ECM component deposition, causing tissue fibrosis and scar formation. Hence, well-balanced activation of fibroblasts was of great significance in reducing scar tissue formation during wound healing. It is well known that transforming growth factor–β1 (TGFβ1) is the most effective cytokine that induces fibroblasts to differentiate into myofibroblasts. The physical and chemical cues of an ECM microenvironment including stiffness and cell adhesion ligand could also promote the fomation of myofibroblasts. However, recent studies have suggested that changes in cell morphology and cytoskeleton tension can be independent of the mechanical properties of the matrix and directly affect the phenotype differentiation of fibroblasts (*17*). Our study has revealed the great influence of topological structure on cell morphology and remodeling of cytoskeleton. It was also reported that the alignment topological structure of matrix can significantly reduce the cytoskeleton tension (*24*). To investigate the effect of topological structure on phenotypic differentiation, immunofluorescence staining of α-SMA staining was carried out (Fig. 5). As reported previously, α-SMA was diffused in cytoplasm under the quiescent fibroblast while formed stress fibers upon differentiation of fibroblasts into myofibroblasts (*25*, *26*). The percentage of activated α-SMA cells in each group was calculated by manual counting (*26*). As shown in Fig. 5A, the F-actin cytoskeleton was significantly remodeled and elongated in cells cultured on the anisotropic fiber matrix compared with irregularly arranged cytoskeleton on random fibers. Both ASCF and RSCF exhibited a COL-I blending ratio–dependent increase of red fluorescent signal representing α-SMA, with fibers containing higher ratios of COL-I (20, 25, and 50%), producing the strongest signal and the integration of α-SMA stress fibers and F-actin indicated by the merging of green and red signal (Fig. 5, A and B). Under the same COL-I ratio, ASCF induced a significantly lower expression of α-SMA (Fig. 5A), compared with RSCF. Red signal could hardly be seen in cells cultured on ASCF containing fewer COL-I (5, 10, and 15%), while in comparison, distinctive expression of α-SMA could be clearly identified on RSCF with same COL-I ratios (Fig. 5A: RSCF, 80:20; 75:25; and 50:50). To quantitative analyze the activation condition of α-SMA, cells with α-SMA integrated with F-actin fiber showing a coincident yellow signal was counted and calculated on different fibers. Under the same COL-I ratio, all groups with anisotropic structure produced a significantly lower activation ratio

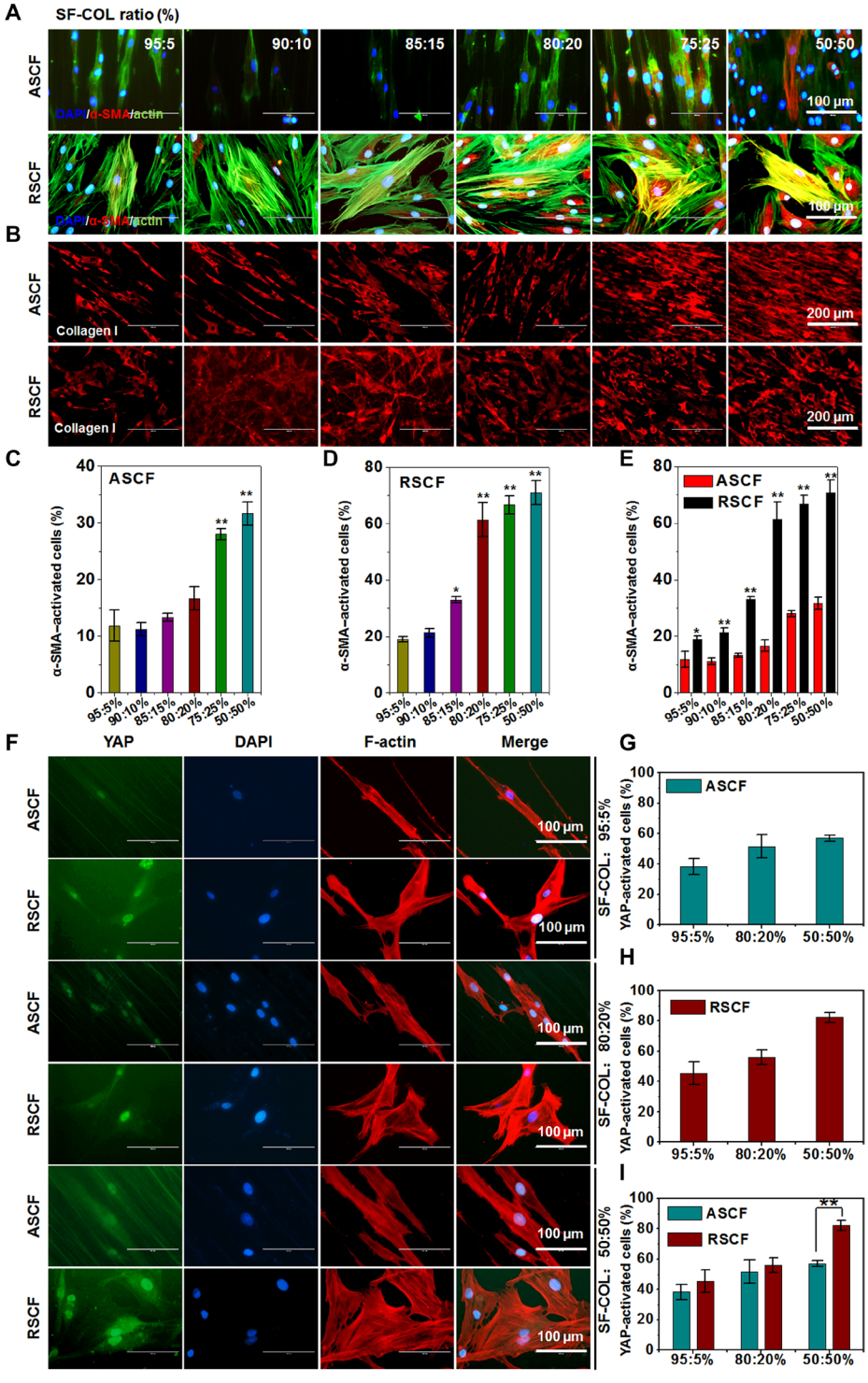

Fig. 5. The influence phenotype and function of fibroblasts by heterogeneous micro/nanofibers and anisotropic topology could suppress YAP activity. (**A**) Immunofluorescence staining of α-SMA in fibroblasts on ASCF and RSCF containing gradient COL-I content. (**B**) Immunofluorescence staining of COL-I in fibroblasts on ASCF and RSCF containing gradient COL-I content. (**C** and **D**) Quantitative analysis of α-SMA activation rate of fibroblasts cultured on (C) ASCF and (D) RSCF containing gradient COL-I content. (**E**) Comparison of α-SMA activation rate between ASCF and RSCF under the same COL-I content. Statistically significant differences were indicated by $^{*}P < 0.05$ and $^{**}P < 0.01$ compared with the 95:5% group (C and D); statistically significant differences were indicated by $^{*}P < 0.05$ and $^{**}P < 0.01$ when comparing between ASCF and RSCF groups (E). (**F**) Immunofluorescence assay of YAP expression and activation. Immunofluorescence staining of YAP in fibroblasts cultured on ASCF and RSDF containing varying COL-I content (5, 20, and 50%). (**G** to **I**) Comparison on YAP activation rate of fibroblasts on ASCF (G) and RSCF (H) and comparison of YAP activation rate between ASCF and RSCF under the same COL-I content (5, 20, and 50%) (I). Statistically significant differences were indicated by $^{*}P < 0.05$ and $^{**}P < 0.01$ compared with the 95:5% group; statistically significant differences were indicated by $^{**}P < 0.01$ when comparing between ASCF and RSCF groups.

of α-SMA compared with random fibers groups (Fig. 5, C to E), consistent with previous studies showing that the orientated nanostructure could inhibit the expression level of α-SMA and reduce scars (*11*, *27*). Our study also showed that the anisotropic electrospun fiber matrix could reduce the expression of α-SMA and inhibit the differentiation of fibroblasts into myofibroblast phenotype.

As one of the main components of ECM, COL-I is secreted by fibroblasts and plays a key role in tissue healing and scar tissue formation. The microstructrure of collagen type I fibers varied distinctively in different tissues such as bone, tendon, ligament, and dura mater and showed high hierarchy and heterogeneity. Production of COL-I from fibroblasts was characterized by immunofluorescence staining. As shown in Fig. 5B, the COL-I produced by fibroblasts on the anisotropic nanofibers exhibited significantly oriented distribution, while the collagen matrix produced by the cells on the random fiber matrix is disordered, indicating that the topology of the electrospun matrix has an important effect on the secretion and remodeling of the ECM. With an increased ratio of COL-I in the scaffold, the fluorescence expression of COL-I in both ASCF and RSCF scaffolds increased obviously, indicating that the chemical cues of the nanofibers also had a great influence on the production of ECM. As activated fibroblasts transformed into myofibroblast phenotype, it could produce more ECM components such as COL-I by accelerating cell proliferation and lead to formation of tissue fibrosis if persistent activation was not properly modulated.

Activation of YAP and myofibroblast phenotype

Recent studies have revealed the transcriptional coactivating factor YAP in the Hippo signaling pathway as a mechanotransduction signal that mediates myofibroblast activation and plays an important role in the differentiation of fibroblasts into myofibroblasts. YAP has also been reported as a major signaling molecule at downstream of integrin β1 and regulator of the myofibroblast phenotype (*13*). Previous studies have shown the effect of cytoskeleton stress fibers and cell morphology on YAP activity, cell proliferation, and differentiation (*14*). In this study, we found that the topological structure of the electrospun fiber could significantly affect the morphology of fibroblast and elongate and remodel the cytoskeleton. The COL-I blending ratio was also revealed to have a significant impact on cell morphology and F-actin distribution and promotes the differentiation of fibroblast into myofibroblast. Therefore, we have inferred that the topological and chemical cues of matrix materials that regulated the morphology and skeleton remodeling of the fibroblasts could also promote the nuclear localization and activation of YAP and contribute to the phenotype differentiation.

In this study, anisotropic and random fiber matrices with COL-I ratios of 5, 20, and 50% were used to study the effect of topological cues on myofibroblast differentiation. Since the translocation of YAP from cytoplasm to nucleus indicated the activation of this molecule, YAP immunofluorescence staining was applied to observe the localization of YAP in cytoplasm and nucleus, with the positive ratio of YAP-activated cells calculated. The morphological profiles of cell and nuclei were also observed on the basis of F-actin phalloidin and 4′,6-diamidino-2-phenylindole (DAPI) staining. As shown in Fig. 5F, the cytoskeleton of the fibroblasts cultured on random fiber matrix was well spreading with a larger spreading area, and YAP was expressed in most of the cells and mainly located in the cell nucleus. No significant differences on YAP activation could be found under lower COL-I content (5 and 20%). However, at COL-I ratio of 50%, the significant higher activation rate could be found on random fibers compared with anisotropic ones. The proportion of YAP-activated cells was calculated to be 82.2 ± 3.3% on random fibers (Fig. 5, G and H). On the anisotropic fiber matrix, the cytoskeleton of fibroblasts was elongated, exhibiting a smaller spreading area, as well as a significantly smaller proportion of YAP-activated cells (57.0 ± 2.0%) compared with that of the random fiber matrix ($P < 0.001$) (Fig. 5I). On the basis of such difference, it is reasonable to believe that the topological and chemical cues of the electrospun fiber matrix could alter the adhesion state of the cells, affect the distribution and remodeling of the skeleton, and exert an obvious influence on the activation of YAP. On the other hand, we could also conclude that the activation and nuclear localization of YAP could lead to one of the pathways guiding the differentiation of fibroblasts into myofibroblasts.

Fabrication of heterogeneous bilayered electrospun fibrous platforms

Through the above experiments, we have verified the effect of different microstructural and chemical cues of electrospun fiber scaffolds on cell behavior. SF/COL-I fiber scaffolds with anisotropic topology was revealed to be beneficial to cell adhesion, regulate cell skeleton remodeling, maintain the spindle shape of fibroblasts, promote cell proliferation, and, more importantly, inhibit the differentiation of fibroblasts into myofibroblast phenotype and prevent fibrosis. By regulating the density of SF-electrospun fibers, the adhesion state of myofibroblast can be changed, with corresponding spreading and proliferation effectively inhibited. The dura mater consisted of large amounts of collagen fibers, elastic fibers, and spindle-shaped fibroblasts. The collagenous fibers within dura were characterized by great diversity on fiber diameter and high structural heterogeneity with the longitudinal collagen fibers arranged in parallel and fibrous fibers distributed irregularly and interwoven with each other (*3*). Therefore, inspired by the heterogeneous microstructure in dura mater, we have combined the effects of micro/nanotopology and biochemical cues to construct a double-layer heterogeneous scaffold to mimic the natural architecture of dura mater and promote the regeneration of spinal dura and prevent the formation of scar tissue.

Characterization of heterogeneous bilayers of electrospun fibrous scaffolds

Microstructure and morphology

SEM was performed to observe the cross-sectional and surface fiber morphology of bilayer scaffolds (Fig. 6A). The inner layer containing ASCF or RSCF nanofibers was found with the thickness of around 80 μm, and the outer SF layer with the diameter of around 120 μm was also observed under cross-sectional SEM views (Fig. 6A, b and e). Both the inner and outer surfaces of the double-layer scaffolds were observed under SEM, which showed a compact and aligned fiber microstructure in the ASCF inner layer (Fig. 6A, a), and a disorderly distribution and interwoven fiber network with larger pores was found on the surface of RSCF inner layer (Fig. 6A, d). The diameters and pore sizes of random or oriented electrospun fibers were uniform, and there was no bead-like structure in the fibers. The diameter of nanofibers was measured to be 474 ± 66 and 484 ± 71 nm in ASCF and RSCF inner layers, respectively, and the diameter of 865 ± 14 nm was found in the SF outer layer (Fig. 6A, c and f). Uniform fibers could be found in all groups without the appearance of a bead-like structure in the fibers.

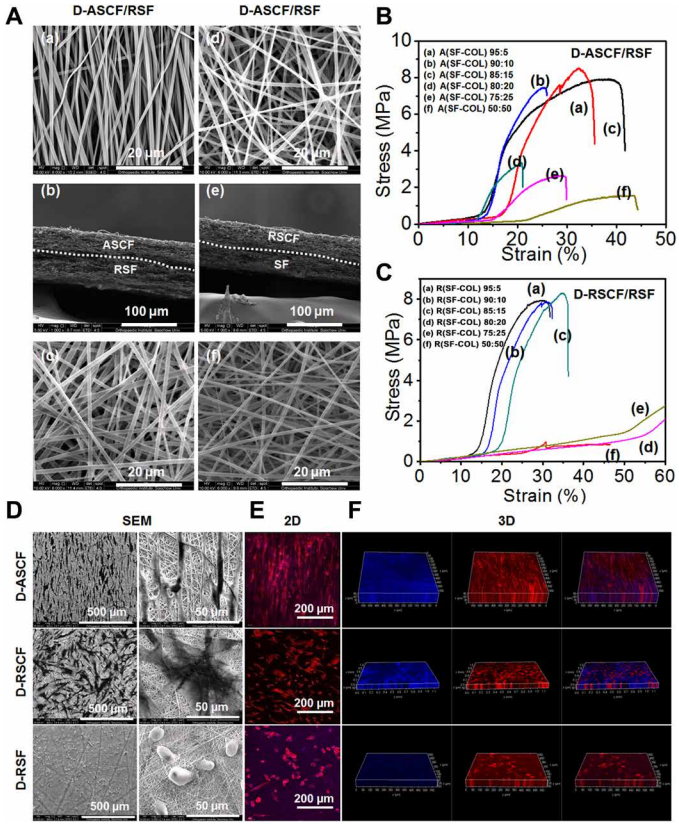

Fig. 6. Physical property and biological function of the dual-layer heterogeneous fiber scaffold. SEM and mechanical characterization of the dual-layer heterogeneous fiber scaffold. (**A**) Morphology of the inner layer (a and d), transverse section layer (b and e), and outer layer of heterogeneous scaffold (c and f). (**B** and **C**) Stress-strain curve of (B) D-ASCF/RSF and (C) D-RSCF/RSF under uniaxial tensile test. Biological evaluation of the dual-layer heterogeneous scaffold. (**D** to **F**) Representative (D) SEM and (E) confocal microscopy images of the cell morphology and cytoskeleton on the inner (D-ASCF and D-RSCF) and outer layers (D-RSF) of the dual-layer heterogeneous scaffold, followed by (F) the 3D reconstruction of cytoskeleton organization.

Mechanical properties

The mechanical properties of the bilayer scaffold were characterized through a tensile test. As shown in Fig. 6 (B and C), all fiber scaffolds exhibited a stress-dependent strain curve. The tensile strengths of fiber scaffolds with various collagen ratios (5, 10, 15, 20, 25, and 50%) were found to be 8.50 ± 0.31, 7.36 ± 0.28, 8.50 ± 0.38, 3.56 ± 0.30, 2.58 ± 0.19, and 1.56 ± 0.23 MPa for D-ASCF/RSF and 7.90 ± 0.16, 7.36 ± 0.28, 8.12 ± 0.31, 2.60 ± 0.34, 2.52 ± 0.15, and 1.56 ± 0.23 MPa for D-RSCF/RSF, respectively, with the elongation rate of 40.40 ± 7.23, 37.40 ± 2.30, 50.40 ± 5.50, 27.20 ± 4.21, 32.00 ± 3.16, and 39.80 ± 2.86% for D-ASCF/RSF and 40.40 ± 7.23, 37.40 ± 2.30, 50.00 ± 5.24, 62.40 ± 5.55, 65.40 ± 4.34, and 44.20 ± 2.49% for D-RSCF/RSF, respectively. With the COL-I ratio in the inner layer reaching 20%, a marked decrease on the maximal tensile strength could be identified on both D-ASCF/RSF and D-RSCF/RSF scaffolds. According to the above characterization, we could conclude that the increase of collagen content would significantly affect the mechanical properties of the scaffolds, and indicated by the results of tensile strength and elongation rate at break, the 15% COL-I ratio was adopted as the optimized value for further characterization due to its acceptable tensile strength and elongation rate. Combined with the results from biological function evaluation, the double-layer heterogeneous scaffold was constructed using an inner layer with a Col-I ratio of 15% and an outer layer with an electrospinning time of 3 hours due to the good mechanical and biological properties of this combination and was further studied in following characterization.

Biological properties

To verify the adhesion and morphology of different cells on the dual-layer heterogeneous scaffold, cells were seeded on both the inner and outer layers of the scaffold and subjected to SEM observation (Fig. 6D) and F-actin cytoskeleton staining (Fig. 6, E and F) after culturing for 24 hours. SEM images indicated that fibroblasts were uniformly distributed on all layers while showing distinct morphology on different layers. The fibroblasts on the inner anisotropic layer elongated and extended along the orientated fibers. In comparison, fibroblasts that adhered on the inner random layer displayed flat and well-spreading morphology that extended to different directions with the appearance of a wide lamellipodium. The outer layer consisted of RSF, on the other hand, hindering the adhesion of myofibroblasts, which exhibited spherical shapes without obvious membrane protuberances and pseudopodium formation. Confocal microscopy 3D images were reconstructed to investigate the capability of different layers to induce cellular infiltration. As shown in Fig. 6F, the fibroblasts were able to infiltrate into the inner layer of the bilayer scaffold, regardless of anisotropic or irregular architecture, while myofibroblasts grew only on the surface of the outer SF layer, indicating the barrier effect of outer layer on cellular infiltration.

Heterogeneous bilayered electrospun fibrous scaffolds for the regeneration of dura mater

Animal surgery

The procedure for the operation of the spinal laminectomy animal model for creating a dural defect was demonstrated in Fig. 1C. A 3 × 11–mm size defect in the central area of the spinal dura was created and covered with a double layer of D-RSCF/RSF or D-ASCF/RSF electrospun membranes over the edge of defect (fig. S7A).

Magnetic resonance imaging evaluation in vivo

Magnetic resonance imaging (MRI) was used to observe the repair of dura mater, the degree of scar adhesion, and fibrosis of epidural tissue 8 weeks after operation. As shown in fig. S7B, abnormal signal could be hardly observed in the spinal, dura, and epidural tissue of the normal control group on the sagittal and transected T2-weighted images. In the control group without implants, because of the tissue structure disorder that resulted from the dura defect, tissue deformation and severe scar fibrosis in the laminectomy area could be observed. The local scar fibrous tissue was found to immerse in the spinal canal with a hardly recognizable boundary between scar tissue and spinal cord, indicating the severely compromised condition of the spinal cord tissue and its functionality. The MRI T2-weighted image showed the characteristic rough high signal. As for the D-RSCF/RSF and D-ASCF/RSF double-layer scaffold implant group, the T2-weighted sagittal and cross-sectional MRI image exhibited a relatively medium or low signal and a clear gap between the epidural and the surrounding tissue, indicating the limited infiltration of the epidural scar tissue in the spinal canal. Assisted by adhesion grading score based on an MRI image, significantly lower adhesion scores were found on the D-RSCF/RSF and D-ASCF/RSF double-layer scaffold compared with the untreated group. No significant difference in the

score between D-RSCF/RSF and D-ASCF/RSF could be found (fig. S7C).

General observation and evaluation

After MRI examination, rabbits were euthanized to obtain the whole spinal tissue specimens containing the surgical segment for the investigation of dura mater regeneration and adhesion between the dura tissue and the surrounding tissue. The gross tissue score of the epidural tissue adhesion in the double-layer scaffold treatment group was significantly lower than that in the nonimplant group, while no significant difference in the gross tissue score could be found between the D-RSCF/RSF and D-ASCF/RSF groups ($P > 0.05$) (Fig. 7E). It was worth noting that a severe scar adhesion between the dura defect and the surrounding tissue was found in the group without the material implantation.

Histopathological examination

Hematoxylin and eosin (H&E) and Masson's trichrome staining were performed to evaluate the generation of dura mater 8 weeks after the operation. As shown in Fig. 7 (A and B), no newborn dura tissue formation could be found, and extensively dense fibrous scar tissue occupied the area of laminectomy accompanied by severe arachnoiditis in the control group without scaffold implantation. In the treatment groups receiving D-RSCF/RSF or D-ASCF/RSF fibrous scaffolds, different degrees of newborn collagen tissue ingrowth could be evidenced in the dura tissue defect area. In the group treated with D-RSCF/RSF scaffolds, irregular and discontinuous newly formed collagen membranes that resembled the scar fibrosis tissue were observed to scatter in surgical areas. On the contrary, continuous collagen tissue was observed in the dura defect area implanted with D-ASCF/RSF scaffold, showing high similarity to normal dura tissue. The newborn collagen tissue extended to the edge of the defect and integrated with the normal dura tissue, leaving an ambiguous boundary between them. On the other hand, both D-RSCF/RSF and D-ASCF/RSF fibrous scaffolds exerted significant influences on preventing epidural scar formation. Histopathological examination results showed that no dense scar fibrotic tissue was formed in the laminectomy area with the epidural space filled with loosen and fat-like tissue, indicating the barrier effect of the bilayer fibrous scaffold on the inhibition of the epidural scar formation. The pathological adhesion at a focal area was also scored to quantify the adhesion condition as shown in Fig. 7F, and significantly lower scores could be found in groups implanted with D-RSCF/RSF and D-ASCF/RSF.

Immunohistochemical examination

The immunohistochemical analysis of α-SMA and COL-I in the epidural tissue was introduced to further verify the effect of the bilayered fibrous scaffolds on preventing epidural scar adhesion. In the untreated control group, dense type I collagen was found in the epidural tissue with a corresponding immunohistochemical image showing strongly positive staining, while on the other hand, collagen distribution resembling normal epidural tissue could be found in D-ASCF/RSF and D-RSCF/RSF groups with a significantly lower expression of type I collagen compared with the control group (Fig. 7, C and G). In addition, the number of α-SMA–positive fibroblasts decreased significantly in D-ASCF/RSF and D-RSCF/RSF groups compared with the control group, while no statistical difference was found between the D-ASCF/RSF and D-RSCF/RSF groups (Fig. 7, D and H). In the control group, a large number of α-SMA–positive fibroblasts were found to cluster at the edge of the wound or around the blood vessels (Fig. 7D). Corresponding quantification also revealed a similar trend (Fig. 7H). According to the results of immunohistochemical analysis, it could be inferred that the anisotropic inner structure of the heterogeneous bilayered fibrous scaffold could promote the regeneration of the dura tissue, while the outer microstructures supported by electrospun SF microfibers effectively inhibited the adhesion and proliferation of the myofibroblasts in the laminectomy area and reduced the number of α-SMA–positive fibroblasts so as to prevent excessive deposition of ECM components and inhibit scar formation and fibrosis in the epidural tissue.

DISCUSSION

Considering the key roles of microstructures, chemical cues, and mechanical properties of the ECM in regulating the function of cells and tissues, increasing designs of biomimetic electrospun scaffolds have emerged to mimic natural ECM for regeneration of various connective tissues such as skin, tendons, and ligaments and prevention of diseases. In this study, we have constructed a heterogeneous dual-layer nanofiber scaffold using silk fibroin and collagen I and demonstrated its effectiveness on promoting fibroblast adhesion and growth. The topological microstructure of an electrospun substrate could modulate cell morphology and further regulate the phenotypic differentiation of fibroblasts. Meanwhile, increased density of SF fibers was revealed to inhibit the adhesion and growth of contractile myofibroblasts. On the basis of these phenomena and inspired by the ECM properties of dura mater, we further assembled the SF/COL-I, SF-electrospun fibers into a bilayer scaffold with heterogeneous topological and chemical properties. The inner layer of the scaffold that consisted of anisotropic SF/COL-I nanofibers promoted the regeneration and repair of the dura mater, while the outer layer constructed with random SF microfibers with optimized fiber density could inhibit the adhesion and proliferation of myofibroblast and prevent the formation of scar fibrosis in epidural tissue. The biomimetic designed scaffolds could satisfy the multiple functional demands during the regeneration and repair of dura tissue.

Increasing evidences have demonstrated that cells can perceive chemical cues and topographical microstructures to regulate adhesion, cytoskeleton remodeling, migration, proliferation, and phenotype differentiation via integrin-mediated interaction of cell matrix (*12*, *28*, *29*). As the major mediator of mechanotransduction, an integrin could deliver the information of ECM stiffness and cytoskeleton tension into the nucleus to regulate gene expression. In this study, we have developed SF/COL-I–blended nanofibers with heterogeneous property. With the increase of collagen composition in nanofibers, the integrin ligand density also increased, which could significantly promote fibroblasts adhering to nanofibers. Silk fibroin is a natural high-molecular protein extracted from silkworm cocoons. Because of its good biocompatibility and excellent mechanical properties, SF has been widely used in tissue engineering research as a scaffold material (*23*). However, owing to the absence of cell-adhesive motifs, supplementing other natural polymers such as gelatin or collagen for enhancing its bioactivity has been found to considerably improve the performance of SF (*30*, *31*). As the most important fibrous structural component of ECM, COL-I provides not only a mechanical microenvironment for cell growth but also a variety of molecular recognition motifs such as RGD, GFOGER, and GVMGFO in its triple-helical structure, responsible for the activation of transmembrane integrin receptors on cell surface including integrins α1β1, α2β1, α10β1, and α11β1 (*32*). The binding of recognition

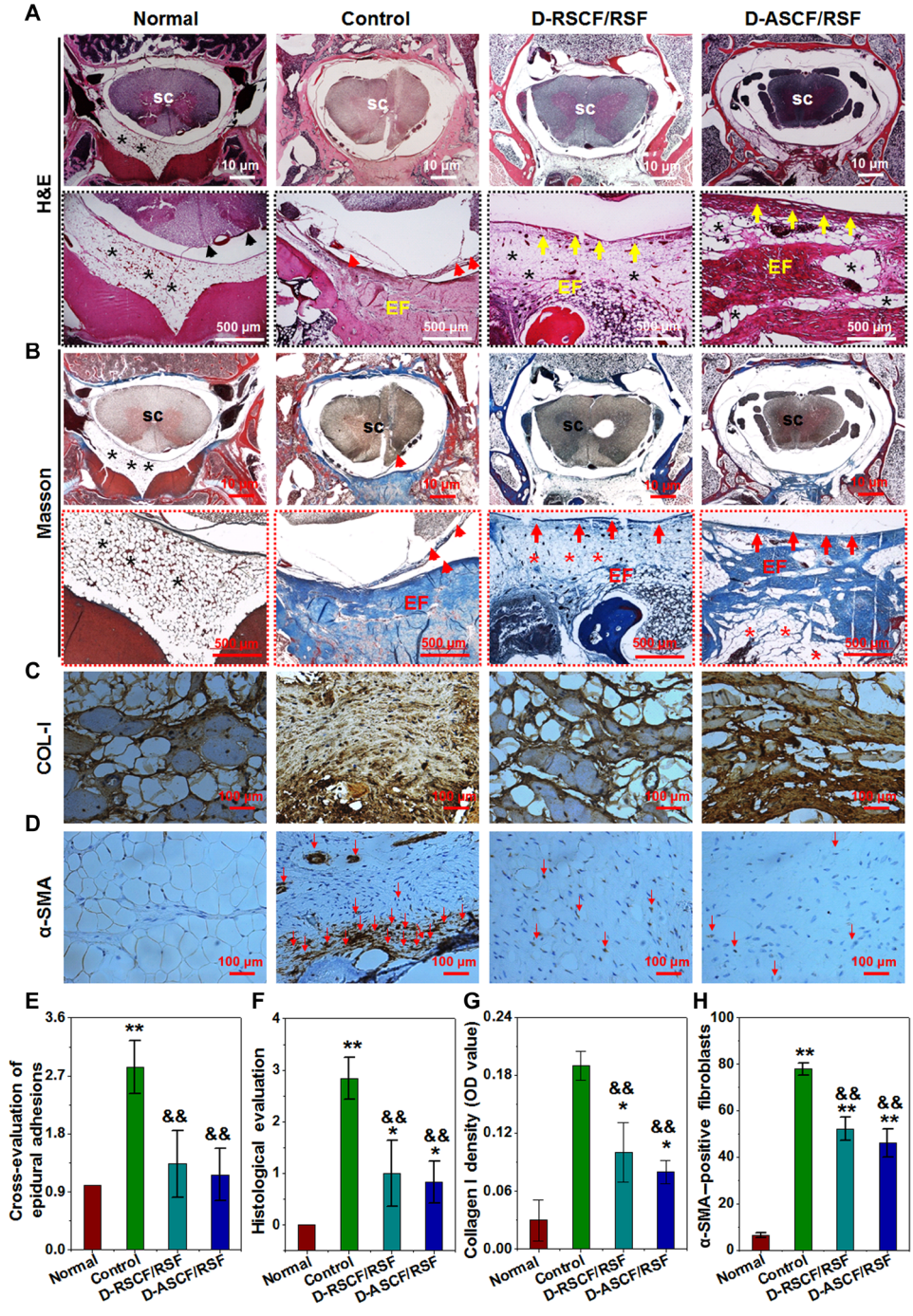

Fig. 7. Histopathological characterization of spinal dura mater and epidural tissues 8 weeks after operation. SC, spine cord; EF, epidural fibrosis. The red arrowhead indicates the spinal arachnoiditis. The black asterisk indicates epidural fat. The red arrow indicates neodura tissue. (**A** and **B**) Histological observation of (A) hematoxylin and eosin (H&E) staining and (B) Masson's trichrome staining at the defect site. (**C** and **D**) Immunohistochemical staining of (C) COL-I and (D) α-SMA at the focal area. (**E** to **H**) Gross evaluation of epidural adhesion (E), histological evaluation (F), relative collagen I density (G), and α-SMA activating quantification of epidural fibrosis (H). Statistically significant differences were indicated by $^{*}P < 0.05$ and $^{**}P < 0.01$ when compared with the normal group and $\&\&P < 0.01$ when compared with the control group. Data are expressed as means ± SD for six samples per group. OD, optical density.

motif from collagen molecular to the extracellular domain of integrin head initiates the classical pathway called outside-in integrin signaling to regulate integrin activation and clustering.

In the current study, we have shown that the activated integrin β1 increased significantly with the increase of collagen ratio in SF/COL-I–electrospun nanofibers, which was consistent with previous studies (*33*). The activated integrin recruits many adaptor proteins such as vinculin, talin, and paxillin to form FA complexes, which was connected to cytoskeleton actin and further responsible for the activation of FAK signaling, followed by the activation of multiple

intracellular signal cascades so as to affect the spreading, proliferation, and phenotypic differentiation of cells (*29*, *34*). The change of cell-matrix interaction modulated by substrate topology could also affect the activation of integrin and the formation of adhesion complexes and, further, to regulate dynamic actomyosin contractile force and cytoskeleton tension. Our results revealed that the anisotropic topological microstructure of the electrospun fiber could inhibit the activation integrin β1 in fibroblasts compared with isotropic nanofibers. The discrepancy could be ascribed to many factors; the nonwoven interlaced porous structure of the random fibers provided more contact sites to increase the density of integrin ligands for cell-matrix interaction. With regard to anisotropic nanofibers, the effect of contact guidance limited the lateral spreading of fibroblasts and changed the space distribution of integrin ligands to hinder integrin clustering and activation.

Cell morphology changes were believed to be highly associated with cell proliferation. Previous studies illustrated that topographical cues such as aligned nanogrooved substrate and carbon nanotubes could modulate cell shape and suppress fibroblast proliferation (*27*). On the other hand, studies have reported a significant synergistic stimulating effect on cell proliferation and differentiation from the topological and chemistry cues of bioscaffolds (*35*). In this study, with the increase of COL-I proportion, an up-regulated cell proliferation could also be found on both anisotropic and random fiber scaffolds, indicating the important role of chemical cues of substrates on supporting the cell adhesion and proliferation, consistent with previous findings (*16*). With the chemical factors well balanced, the anisotropic topology was reported to significantly down-regulate the proliferation rate of fibroblast compared to isotropic topology. Accordingly, our data have shown similar trends on anisotropic topology affecting fibroblast proliferation. SEM images and F-actin staining have provided further evidence on the effect of anisotropic topology, showing critical difference on the morphology of cells on random and alignment fibrous matrix as well as the rearrangement of cytoskeleton due to the contact guidance. In addition, immunofluorescence staining indicated that vinculin was confined to the cytoplasm without significant formation of a punctate-like FA in the end of cells seeded on anisotropic topology, which reflected the loose contact between cells and the matrix. Therefore, we conclude that the anisotropic topological microstructure of nanofibers suppressed fibroblast proliferation by modulating cell morphology and inhibited FA mature.

In this study, silk fibroin is a safe and stable nature polymer, which can be used to fabricate ECM-like fibrous substrates and to investigate its capability to affect fibroblast behaviors and promote dura regeneration and fibrosis inhibition. The density of SF fibers was customized through adjusting collecting time during electrospinning to regulate the adhesive morphology and proliferation of myofibroblasts. Myofibroblast morphology underwent a gradual alteration from fully spreading morphology to spheroid along with the increase of fiber density. Subsequently, the proliferation rate of myofibroblasts decreased significantly upon denser fibers. Recently, studies illustrated that increasing stiffness of fibrous substrate could suppress adhesion, spreading, and proliferation of fibroblasts (*36*). Here, it could be inferred that the increase of fiber density could decrease the pore size of fibrous membrane and subsequently increase the overall stiffness, both of which would affect the adhesion and proliferation of myofibroblasts. In addition, the biological inertness of SF protein relative to other natural polymers also contributed to this suppression effect. Together, SF fibers with optimized density could direct cell morphology and proliferation, holding great promise for the prevention of myofibroblast infiltration and scar contraction.

Substrate stiffness and TGFβ1 signaling have been considered as important factors regulating the phenotype differentiation of fibroblasts into myofibroblasts. Recently, studies have shown that topographical microstructure and chemical cues of matrix also played important roles in enhancing fibroblast-to-myofibroblast differentiation. Huang *et al.* (*37*) demonstrated that, independent of matrix stiffness and TGFβ1 signaling, anisotropic collagen-containing nanofibers could enhance the differentiation of fibroblasts into myofibroblasts via activating integrin β1 signal and FAK phosphorylation. However, contradictive evidences have also been reported, which suggested the effect of anisotropic topology on maintaining fibroblast quiescent phenotype and effect ECM synthesis (*11*, *27*, *38*). Currently, our results indicated that random SF/COL-I nanofibers up-regulated α-SMA expression in fibroblast upon increasing the COL-I ratio and, more importantly, promoted the integration of F-actin cytoskeleton and stress fiber formation. The anisotropic fibers, on the other hand, inhibited integrin β1 activation and induced limited α-SMA expression under a high COL-I ratio. It could be inferred that the anisotropic topology of SF/COL-I–electrospun nanofibers could inhibit the effect of integrin β1–FAK signal pathway on the phenotype differentiation of myofibroblast and provide new evidences on the association between topological cues and myofibroblast activation.

Despite the antiactivation effect observed in our study, the underlying mechanism involved in the anisotropic topographical structure preserving the quiescent phenotype of fibroblasts remains elusive. Anisotropic topographical structure induces elongated cell morphology, which can reduce cytoskeleton tension and contractile force. On the contrary, well-spread fibroblasts exhibited F-actin cytoskeleton polymerization and, further, stress fiber formation, both of which promoted fibroblast activation and resulted in greater cytoskeleton tension (*17*). Recent studies have suggested the association between α-SMA–mediated fibrosis and YAP signaling, a downstream biomarker of integrin β1 (*13*, *39*). Diverse elements including cell morphology, spreading area, stress fiber formation, and cytoskeleton tension alteration could affect YAP activation deriving from the activation of integrin β1 signal (*40*). Since anisotropic fibrous topographical microstructure changed the space distribution of integrin β1 ligands in substrate, we have found inhibited integrin β1 activation, which could further suppress the activity of YAP signaling. Immunofluorescence staining indeed verified a significantly lower activation rate of YAP on anisotropic fibers as well as elongated morphology and significantly smaller spreading area when compared with random fibers. Therefore, our finding confirmed that the mechanism of the topological and chemical cues regulating the phenotype differentiation of fibroblasts could be mainly associated with the changes on cell morphology, the distribution of the FA, cytoskeleton reorganization, stress fibers, and integrin β1 activation and nuclear localization of the transcriptional coactivating factor YAP. Therefore, we suggest that SF/COL-I–electrospun fibers with anisotropic structure could preserve the quiescent phenotype of fibroblasts.

The specific microenvironment in dura mater defect site after surgery has put forward multiple requirements on designs of regenerative

scaffolds, which should be capable of simultaneously promoting dura regeneration and inhibiting epidural fibrosis. According to a previous study of our group (*41*), the microstructure and functional properties of homogeneous electrospun scaffolds could hardly be competent in treating complicated conditions in dura defect and needed to be further tailored to promote tissue regeneration and to prevent epidural fibrosis. Recent studies indicated that alignment electrospun nanofibers could potentially facilitate the biological healing of wounds and circumvent the risk of scar formation. As a template for tissue healing, the scaffold implanted in vivo should be capable of hindering myofibroblast infiltration and withstanding its contractile force. Otherwise, the collapse and loss of scaffold microstructures due to cell contractile force would compromise tissue healing and aggravate scar fibrosis. Hence, retaining the mechanical integrity of biomaterials in vivo presented an urgent need in tissue regeneration. Park *et al*. (*42*) fabricated the bilayer homogeneous electrospun scaffold containing both aligned fibers and random fibers to provide contact guidance and to reinforce the mechanical stability of scaffolds, respectively, resulting in higher porosity, better dispersion, and better permeability, all of which were essential for the transportation of nutrition and excretion of metabolic waste. A bilayer electrospun scaffold containing anisotropic and random nanofibers has also been reported by Kurpinski and Patel (*43*) for its great advantages in promoting dura mater repair. However, few studies have fully taken the microenvironment of dura mater into consideration, which, as a matter of fact, has high complexity and heterogeneity and requires distinct attributes on different sides of the scaffold. Specifically, the main focus has been concentrated on the regeneration of dura mater that depended on the activity of fibroblasts, which, however, could be a potential threat due to their persistent activation and overproduction of myofibroblasts, leading to the fibrosis of focal tissue. To fit the specific needs, designs of scaffold could be further tuned on physical and chemical properties for better modulation of cell behavior. Therefore, a heterogeneous dual-layer scaffold was fabricated using SF and COL-I and endowed with well-tuned topological and chemical cues so as to accurately regulate fibroblast activation and inhibit epidural myofibroblast activity. The roles of alignment SF/COL-I nanofibers in the inner layer of the scaffold are facilitating cell adhesion and growth, directing cytoskeleton reorganization, maintaining the spindle shape of the cells, and inhibiting the differentiation of fibroblasts into myofibroblasts. The outer SF fibrous layer is a submicrometer nonwoven structure with optimized density and pore size that could not only transport nutrients and metabolic waste but also suppress the adhesion and proliferation of myofibroblasts. The mechanical test of the scaffold results show that the tensile strength of the bilayer scaffold is up to 8 MPa. Therefore, SF random fibers could effectively maintain the integration and stability of scaffolds, inhibit the contraction by myofibroblasts, and reduce scar formation. In an in vivo study, the ECM-inspired scaffolds confirmed the effects of promoting dura mater regeneration and alleviating epidural scar fibrosis in a rabbit laminectomy model. By histopathological examination, we have observed that D-ASCF/RSF scaffolds could effectively promote the regeneration of spinal dural tissue and form a continuous alignment of collagen tissue, similar to the natural dura tissue. On the other hand, disordered and discontinuous regenerated dural tissue could be observed at the implanting site of D-RSCF/RSF. Following immunohistochemistry studies further verified the inhibitory effect of heterogeneous double-layer fiber scaffolds on epidural fibrosis. By reducing the adhesion and growth of myofibroblasts, the secretion of type I collagen and the expression of α-SMA were significantly reduced. However, since both D-ASCF/RSF and D-RSCF/RSF scaffolds have same outer layer composed of dense SF fibers, no significant difference has been evidenced on the expression of collagen I and α-SMA in epidural areas between the two groups.

In conclusion, the dual-layer heterogeneous fiber scaffold constructed to reproduce the microstructure and functionalities of dura mater has demonstrated effective modulation on fibroblast and myofibroblast activities and sufficient mechanical property for practical application. The inner anisotropic fibers with optimized chemical composition were revealed to be able to maintain the quiescent phenotype of fibroblasts while simultaneously allowing for their proliferation and activity, which was essential for dura regeneration. The outer layer, on the other hand, could significantly suppress the adhesion and proliferation of myofibroblasts through increased SF fiber density, inhibiting the development of epidural fibrosis. Further exploration on the mechanism of topological and chemical cues regulating fibroblast phenotype differentiation has revealed the involvement of integrin β1 clustering and the downstream YAP signaling, which will provide further clues in future studies on antifibrosis materials science. Together, the heterogeneous fiber scaffold proved to be efficient and versatile in promoting dura mater functional regeneration and inhibiting epidural scar.

MATERIALS AND METHODS

Preparation of electrospun micro/nanofibers with different topographical structures and compositions

Silk fibroin used in the construction of fiber scaffold was prepared according to the protocol reported previously (*44*). Briefly, the desericin process was carried out through boiling *Bombyx mori* cocoons in aqueous solution of Na_2CO_3 (0.5%, w/w) (Aladdin, Shanghai, China) for 1 hour, followed by thorough washing in deionized water at least eight times. After being fully dried, the desericin SF was dissolved in 9.3 M LiBr at 60°C and further dialyzed for 4 days in a 3500–molecular weight dialysis tube against deionized water, which was changed twice a day. The freeze-dried silk fibroin was obtained through lyophilization of the solution after dialysis.

Freeze-dried SF and COL-I powder (Sigma-Aldrich) were respectively dissolved in 1,1,1,3,3,3-hexafluoro-2-propanol at a concentration of 7%, and the electrospinning solution was prepared by mixing different ratios of SF and COL-I solutions (95:5, 90:10, 85:15, 80:20, 75:25, and 50:50%). A cylindrical collector with a diameter of 8 cm was covered with aluminum foil to collect the electrospun fibers. RSCF were collected with the collector rotating speed of 500 rpm and the collector-to-tip distance of 15 cm for 1 hour, while ASCF were collected with the rotating speed of 3000 rpm and the collecting distance of 10 cm for same amount of time. SF fibers with varying densities were prepared with different collecting times: 30, 60, 120, and 240 s, and 1 and 2 hours. Scaffolds were further cross-linked by placing them in glutaraldehyde steam at room temperature for 12 hours. Scaffolds for cell culture were prepared by attaching uniformly spaced glass coverslips (diameter at 14 mm) onto the aluminum foil to collect electrospun fibers. Nomenclature and abbreviations of the electrospun matrix were provided as follows. The aligned SF/COL-I fiber was abbreviated as

ASCF, the random SF/COL-I fiber was abbreviated as RSCF, and, lastly, the random SF fiber was abbreviated as RSF.

Characterization of electrospun micro/nanofibers

The surface morphological feature was characterized via SEM. Before SEM observation, samples were sputter-coated with gold for 60 s. The observation of samples was conducted under a voltage of 10 kV. The average fibrous diameter and morphological distribution were calculated via quantitative analysis of SEM images.

The chemical characteristics of the scaffold were analyzed via FTIR spectroscopy (Nicolet 6700; Thermo Fisher Scientific, USA). For each measurement, 128 scans were obtained with a resolution of 4 cm^{-1} between 4000 and 400 cm^{-1}.

Cell culture

Human skin fibroblasts and human skin keloid cells were donated by M. Xihuan from Shanghai Ninth People's Hospital. Briefly, the cryovial was moved from the liquid nitrogen to a 37°C water bath and gently shaken for rapid thawing. Thawed cell suspension was aspirated into a centrifuge tube with 10 ml of cultural medium and further centrifuged at 1000 rpm for 5 min. After removing the supernatant, cells were resuspended with Dulbecco's modified Eagle's medium (DMEM) and seeded in a 10-cm petri dish. The culture plate was placed in an incubator at 37°C and 5% CO_2, with the culture medium changed every 2 days. Cells were passed upon reaching the confluence rate of 90%.

Cell seeding

Round glass slides bearing different fibers were placed on the bottom of 24-well plates and sterilized with 75% ethanol for 1 hour, followed by ultraviolet irradiation for 30 min. The scaffolds were soaked in the high-glucose medium (DMEM) containing 10% fetal bovine serum overnight before cell seeding. For the characterization of ASCF and RSCF scaffolds, fibroblasts were seeded at a density of 1×10^4 per well and further cultured at 37°C and 5% CO_2. For the characterization of the SF fiber scaffold, myofibroblasts were seeded with the same density and cultured under the same condition.

Flow cytometry

Flow cytometry was conducted on fibroblasts that were cultured on various fiber scaffolds. After digesting and washing from scaffolds, cells were centrifuged and resuspended at a concentration of 1.0×10^7/ml and further incubated with anti-human anti–integrin β1 antibody (clone HUTS-4) for 30 min at 4°C. After incubating with a secondary fluorescent antibody [goat anti-mouse fluorescein isothiocyanate (FITC)] for 10 min, the cells were subjected to flow cytometry.

Scanning electron microscopy

Cells cultured on fiber scaffolds were fixed with 4% paraformaldehyde at 4°C for 30 min. Ethanol dehydration (10, 20, 35, 50, 70, 85, and 100%) was conducted on samples, followed by critical point drying for 4 hours. After coating with gold for 100 s, field-emission SEM observation was carried with an accelerating voltage of 10 kV.

Cytoskeleton (F-actin) staining

Cells seeded on scaffolds were fixed with paraformaldehyde at room temperature for 10 to 15 min. After rinsing three times with phosphate-buffered saline (PBS), samples were treated with PBS containing 0.1% Triton X-100 and further blocked with 4% bovine serum albumin. Staining was conducted using phalloidin (1:300 dilution; Sigma-Aldrich) for 40 min and DAPI (1:300 dilution) for 10 min and observed under a fluorescence microscope.

Cell spreading and proliferation

Cell spreading area of fibroblasts or myofibroblasts on different scaffolds was quantified on the basis of the SEM images using ImageJ software. Cell proliferation condition was characterized after seeding cells on different scaffolds for certain periods of time. CCK-8 was used to quantify the proliferation rate.

Immunofluorescence staining

With the help of immunofluorescence staining, expression of integrin β1 and vinculin was detected 12 and 24 hours after seeding, respectively, while the activation of α-SMA and the nuclear localization of YAP in fibroblasts were characterized after 3 days of culture. Briefly, after fixing in 4% paraformaldehyde solution at 4°C for 30 min, samples were rinsed three times and treated with 0.1% Triton X-100 for 10 min at room temperature. After blocking with 2% bovine serum albumin at 4°C overnight, samples were stained against primary anti-murine anti-vinculin monoclonal antibody (1:200 dilution), anti–integrin β1 antibody (1:200 dilution), α-SMA monoclonal antibody (1:300), anti-YAP antibody (1:200 dilution), and anti–type I collagen antibody (1:200 dilution), respectively, at 4°C overnight, followed by the incubation of secondary antibody [goat anti-mouse immunoglobulin G (IgG) (H ± L) Cy3 (1:300 dilution) for vinculin, collagen I, integrin β1, and α-SMA; goat anti-rabbit IgG (H ± L) FITC (1:300 dilution) for YAP] at 37°C for 1 hour. After washing twice with PBS, F-actin and nuclei were respectively stained with phalloidin and DAPI. Observation and photography were carried out with a fluorescence microscope.

Preparation and characterization of heterogeneous bilayer fiber scaffold

Bilayer fibrous scaffolds were prepared according to the sequential electrospinning method reported previously (*45*). Briefly, the SF-electrospun fibers were collected on a cylindrical collector covered with aluminum foil with a rotation speed of 500 rpm and a collecting time of 3 hours to form the outer layer of the bilayer scaffold, after which the SF/COL-I solutions with different COL-I ratios were immediately applied for subsequent electrospinning for 2 hours with the collector to form the ASCF or RSCF, which served as the inner layer of the scaffold. The scaffold with the ASCF as the inner layer and RSF as the outer layer was abbreviated as D-ASCF/RSF, while the scaffold with the random SF/COL-I inner layer and random SF outer layer was abbreviated as D-RSCF/RSF.

Mechanical properties

The mechanical property was characterized with a uniaxial tensile test. Briefly, dumbbell-shaped samples of dual-layer fiber scaffolds were fixed with a customized clip on a universal mechanical test system. The tensile test was conducted with a tensile speed of 0.5 mm s^{-1}, and the stress-strain curves were recorded until the failure of the sample.

Biological properties of bilayer fibrous scaffolds

Both D-ASCF/RSF and D-RSCF/RSF scaffolds were placed in 24-well plates after thorough sterilization. Fibroblasts were seeded on

the inner layer of the scaffold, while myofibroblasts were seeded on the outer layer at a density of 1×10^4 per well. After culturing for 24 hours, samples were fixed with 4% paraformaldehyde and treated with 0.1% Triton X-100 for the staining of F-actin and nuclei using phalloidin and DAPI. Cell morphology and infiltration into scaffolds were observed using confocal microscopy with further 3D reconstruction conducted using Leica software.

Animal surgery

Surgical procedures and postsurgical treatment conducted in this study were in accordance with protocols approved by the Ethics Committee of the First Affiliated Hospital of Soochow University. A rabbit duraplasty model was prepared according to the protocol previously reported by our group (*41*). Briefly, after anesthetizing using pentobarbital (10 mg kg^{-1}), a longitude incision was made and the paraspinal muscles were bluntly striped to expose L5 laminae, followed by a total laminectomy to expose dura mater. A dura defect with a size of 0.3×1.1 cm^2 was created and covered with different scaffolds or left empty as a control. A total of 18 rabbits were divided into three groups to either be scaffold free or receive D-RSCF/RSF or D-ASCF/RSF in the dura defect. In addition, a normal group of six rabbits without surgery was also used as normal control.

Magnetic resonance imaging

Eight weeks after the operation, scanning was performed using a 1.5T GE Signa MRI instrument (Signa HDe; GE Medical Systems, Milwaukee, WI) to evaluate the status of dura mater repair and epidural scar formation. The parameters used in scanning were listed as follows: fast-recovery fast spin echo (FRFSE) FRFSE-XL; repetition time/echo time (TR/TE), 3500/102 ms; echo train length, 8; 320 × 256; slice thickness, 5.0 mm/1.4 mm skip; receiver bandwidth, 12.5 Hz $pixel^{-1}$; number of excitation, 8; and field of view, 15 × 15. Epidural fibrosis was further scored on the basis of MRI images according to the scoring system present in (*46*) (table S1).

Gross observation and histopathological examination

After MRI scan, animals were euthanized by intramuscular injection of excessive pentobarbital. Spinal specimens were harvested from the surgical section with their gross condition observed. Gross evaluation of epidural adhesions was performed using the Rydell-BAalaz standard (table S2) (*47*). After the gross evaluation, the samples were fixed in 10% formalin for 24 hours and further decalcified in 10% formic acid for 1 week at room temperature. After embedding in paraffin, 8-μm-thick slices were prepared and subjected to H&E and Masson's trichrome staining, followed by COL-I and α-SMA immunohistochemical staining to observe the pathological condition at the defect area. Histological evaluation of epidural adhesions at the laminectomy site was assessed according to the scoring system presented in (*48*) (table S3).

Statistical analysis

All experimental data were statistically analyzed and plotted using Origin 8.0 and SPSS 16.0 software and presented as means ± SD. Date difference was analyzed using one-way analysis of variance (ANOVA) and Tukey's analysis. $P < 0.05$ was considered statistically significant.

SUPPLEMENTARY MATERIALS

Supplementary material for this article is available at http://advances.sciencemag.org/cgi/content/full/6/48/eabc2036/DC1

REFERENCES AND NOTES

1. A. D. Theocharis, S. S. Skandalis, C. Gialeli, N. K. Karamanos, Extracellular matrix structure. *Adv. Drug Deliv. Rev.* **97**, 4–27 (2016).
2. W. M. Han, S. J. Heo, T. P. Driscoll, J. F. Delucca, C. M. McLeod, L. J. Smith, R. L. Duncan, R. L. Mauck, D. M. Elliott, Microstructural heterogeneity directs micromechanics and mechanobiology in native and engineered fibrocartilage. *Nat. Mater.* **15**, 477–484 (2016).
3. M. Protasoni, S. Sangiorgi, A. Cividini, G. T. Culuvaris, G. Tomei, C. Dell'Orbo, M. Raspanti, S. Balbi, M. Reguzzoni, The collagenic architecture of human dura mater. *J. Neurosurg.* **114**, 1723–1730 (2011).
4. G. Huang, F. Li, X. Zhao, Y. Ma, Y. Li, M. Lin, G. Jin, T. J. Lu, G. M. Genin, F. Xu, Functional and biomimetic materials for engineering of the three-dimensional cell microenvironment. *Chem. Rev.* **117**, 12764–12850 (2017).
5. C.-S. Kim, J.-H. Kim, B. Kim, Y.-S. Park, H.-K. Kim, H. T. Tran, S. H. Kim, H. Jeon, S. Kim, J. H. Sim, H. M. Shin, G. Kim, Y. J. Baik, K.-J. Lee, H.-Y. Kim, T. J. Yun, Y. S. Kim, H.-R. Kim, A specific groove pattern can effectively induce osteoblast differentiation. *Adv. Funct. Mater.* **27**, 1703569 (2017).
6. J. K. Sahoo, M. A. VandenBerg, M. J. Webber, Injectable network biomaterials via molecular or colloidal self-assembly. *Adv. Drug Deliv. Rev.* **127**, 185–207 (2018).
7. A. Szentivanyi, T. Chakradeo, H. Zernetsch, B. Glasmacher, Electrospun cellular microenvironments: Understanding controlled release and scaffold structure. *Adv. Drug Deliv. Rev.* **63**, 209–220 (2011).
8. G. Yang, X. Li, Y. He, J. Ma, G. Ni, S. Zhou, From nano to micro to macro: Electrospun hierarchically structured polymeric fibers for biomedical applications. *Prog. Polym. Sci.* **81**, 80–113 (2018).
9. K. Wang, L. Liu, J. Xie, L. Shen, J. Tao, J. Zhu, Facile strategy to generate aligned polymer nanofibers: Effects on cell adhesion. *ACS Appl. Mater. Interfaces* **10**, 1566–1574 (2018).
10. N. M. Lee, C. Erisken, T. Iskratsch, M. Sheetz, W. N. Levine, H. H. Lu, Polymer fiber-based models of connective tissue repair and healing. *Biomaterials* **112**, 303–312 (2017).
11. D. Phu, L. S. Wray, R. V. Warren, R. C. Haskell, E. J. Orwin, Effect of substrate composition and alignment on corneal cell phenotype. *Tissue Eng. Part A* **17**, 799–807 (2010).
12. J. Z. Kechagia, J. Ivaska, P. Roca-Cusachs, Integrins as biomechanical sensors of the microenvironment. *Nat. Rev. Mol. Cell Biol.* **20**, 457–473 (2019).
13. K. Martin, J. Pritchett, J. Llewellyn, A. F. Mullan, V. S. Athwal, R. Dobie, E. Harvey, L. Zeef, S. Farrow, C. Streuli, N. C. Henderson, S. L. Friedman, N. A. Hanley, K. Piper Hanley, PAK proteins and YAP-1 signalling downstream of integrin beta-1 in myofibroblasts promote liver fibrosis. *Nat. Commun.* **7**, 12502 (2016).
14. K. Wada, K. Itoga, T. Okano, S. Yonemura, H. Sasaki, Hippo pathway regulation by cell morphology and stress fibers. *Development* **138**, 3907–3914 (2011).
15. E. Vatankhah, M. P. Prabhakaran, D. Semnani, S. Razavi, M. Zamani, S. Ramakrishna, Phenotypic modulation of smooth muscle cells by chemical and mechanical cues of electrospun tecophilic/gelatin nanofibers. *ACS Appl. Mater. Interfaces* **6**, 4089–4101 (2014).
16. Y. Maghdouri-White, G. L. Bowlin, C. A. Lemmon, D. Dreau, Mammary epithelial cell adhesion, viability, and infiltration on blended or coated silk fibroin-collagen type I electrospun scaffolds. *Mater. Sci. Eng. C* **43**, 37–44 (2014).
17. E. K. Yim, E. M. Darling, K. Kulangara, F. Guilak, K. W. Leong, Nanotopography-induced changes in focal adhesions, cytoskeletal organization, and mechanical properties of human mesenchymal stem cells. *Biomaterials* **31**, 1299–1306 (2010).
18. J. J. Tomasek, G. Gabbiani, B. Hinz, C. Chaponnier, R. A. Brown, Myofibroblasts and mechano-regulation of connective tissue remodelling. *Nat. Rev. Mol. Cell Biol.* **3**, 349–363 (2002).
19. E. R. Lorden, K. J. Miller, L. Bashirov, M. M. Ibrahim, E. Hammett, Y. Jung, M. A. Medina, A. Rastegarpour, M. A. Selim, K. W. Leong, H. Levinson, Mitigation of hypertrophic scar contraction via an elastomeric biodegradable scaffold. *Biomaterials* **43**, 61–70 (2015).
20. N. Watanabe, T. Kato, A. Fujita, T. Ishizaki, S. Narumiya, Cooperation between mDia1 and ROCK in Rho-induced actin reorganization. *Nat. Cell Biol.* **1**, 136–143 (1999).
21. P. J. Keely, J. K. Westwick, I. P. Whitehead, C. J. Der, L. V. Parise, Whitehead IP,Der CJ,Parise LV, Cdc42 and Rac1 induce integrin-mediated cell motility and invasiveness through PI(3) K. *Nature* **390**, 632–636 (1997).
22. C. J. Bettinger, Z. Zhang, S. Gerecht, J. T. Borenstein, R. Langer, Enhancement of in vitro capillary tube formation by substrate nanotopography. *Adv. Mater.* **20**, 99–103 (2008).
23. B. Kundu, R. Rajkhowa, S. C. Kundu, X. Wang, Silk fibroin biomaterials for tissue regenerations. *Adv. Drug Deliv. Rev.* **65**, 457–470 (2013).
24. A. Tijore, P. Cai, M. H. Nai, L. Zhuyun, W. Yu, C. Y. Tay, C. T. Lim, X. Chen, L. P. Tan, Role of cytoskeletal tension in the induction of cardiomyogenic differentiation in micropatterned human mesenchymal stem cell. *Adv. Healthc. Mater.* **4**, 1399–1407 (2015).
25. A. M. Kloxin, J. A. Benton, K. S. Anseth, In situ elasticity modulation with dynamic substrates to direct cell phenotype. *Biomaterials* **31**, 1–8 (2010).
26. H. Ma, A. R. Killaars, F. W. DelRio, C. Yang, K. S. Anseth, Myofibroblastic activation of valvular interstitial cells is modulated by spatial variations in matrix elasticity and its organization. *Biomaterials* **131**, 131–144 (2017).

27. W. Weng, S. He, H. Song, X. Li, L. Cao, Y. Hu, J. Cui, Q. Zhou, H. Peng, J. Su, Aligned carbon nanotubes reduce hypertrophic scar via regulating cell behavior. *ACS Nano* **12**, 7601–7612 (2018).
28. R. Changede, H. Cai, S. J. Wind, M. P. Sheetz, Integrin nanoclusters can bridge thin matrix fibres to form cell-matrix adhesions. *Nat. Mater.* **18**, 1366–1375 (2019).
29. M. J. Dalby, N. Gadegaard, R. O. Oreffo, Harnessing nanotopography and integrin-matrix interactions to influence stem cell fate. *Nat. Mater.* **13**, 558–569 (2014).
30. E. S. Gil, B. Panilaitis, E. Bellas, D. L. Kaplan, Functionalized silk biomaterials for wound healing. *Adv. Healthc. Mater.* **2**, 206–217 (2013).
31. B. Marelli, M. Achilli, A. Alessandrino, G. Freddi, M. C. Tanzi, S. Fare, D. Mantovani, Collagen-reinforced electrospun silk fibroin tubular construct as small calibre vascular graft. *Macromol. Biosci.* **12**, 1566–1574 (2012).
32. B. Leitinger, Transmembrane collagen receptors. *Annu. Rev. Cell Dev. Biol.* **27**, 265–290 (2011).
33. B. Zhu, W. Li, R. V. Lewis, C. U. Segre, R. Wang, E-spun composite fibers of collagen and dragline silk protein: Fiber mechanics, biocompatibility, and application in stem cell differentiation. *Biomacromolecules* **16**, 202–213 (2015).
34. Z. Sun, M. Costell, R. Fassler, Integrin activation by talin, kindlin and mechanical forces. *Nat. Cell Biol.* **21**, 25–31 (2019).
35. Z. Wu, Y. Xu, H. Li, Synergetic stimulation of nanostructure and chemistry cues on behaviors of fibroblasts and endothelial cells. *Colloids Surf. B* **160**, 500–509 (2017).
36. B. M. Baker, B. Trappmann, W. Y. Wang, M. S. Sakar, I. L. Kim, V. B. Shenoy, J. A. Burdick, C. S. Chen, Cell-mediated fibre recruitment drives extracellular matrix mechanosensing in engineered fibrillar microenvironments. *Nat. Mater.* **14**, 1262–1268 (2015).
37. C. Huang, X. Fu, J. Liu, Y. Qi, S. Li, H. Wang, The involvement of integrin beta1 signaling in the migration and myofibroblastic differentiation of skin fibroblasts on anisotropic collagen-containing nanofibers. *Biomaterials* **33**, 1791–1800 (2012).
38. L. S. Wray, E. J. Orwin, Recreating the microenvironment of the native cornea for tissue engineering applications. *Tissue Eng. Part A* **15**, 1463–1472 (2009).
39. T. Panciera, L. Azzolin, M. Cordenonsi, S. Piccolo, Mechanobiology of YAP and TAZ in physiology and disease. *Nat. Rev. Mol. Cell Biol.* **18**, 758–770 (2017).
40. M. C. Schroeder, G. Halder, Regulation of the Hippo pathway by cell architecture and mechanical signals. *Semin. Cell Dev. Biol.* **23**, 803–811 (2012).
41. Y. Xu, W. Cui, Y. Zhang, P. Zhou, Y. Gu, X. Shen, B. Li, L. Chen, Hierarchical micro/nanofibrous bioscaffolds for structural tissue regeneration. *Adv. Healthc. Mater.* **6**, 1601457 (2017).
42. S. H. Park, M. S. Kim, B. Lee, J. H. Park, H. J. Lee, N. K. Lee, N. L. Jeon, K. Y. Suh, Creation of a hybrid scaffold with dual configuration of aligned and random electrospun fibers. *ACS Appl. Mater. Interfaces* **8**, 2826–2832 (2016).
43. K. Kurpinski, S. Patel, Dura mater regeneration with a novel synthetic,bilayered nanofibrous dural substitute: An experimental study. *Nanomedicine* **6**, 325–337 (2011).
44. X. Shen, Y. Zhang, Y. Gu, Y. Xu, Y. Liu, B. Li, L. Chen, Sequential and sustained release of SDF-1 and BMP-2 from silk fibroin-nanohydroxyapatite scaffold for the enhancement of bone regeneration. *Biomaterials* **106**, 205–216 (2016).
45. S. Liu, J. Zhao, H. Ruan, T. Tang, G. Liu, D. Yu, W. Cui, C. Fan, Biomimetic sheath membrane via electrospinning for antiadhesion of repaired tendon. *Biomacromolecules* **13**, 3611–3619 (2012).
46. C. Li, H. Wang, H. Liu, J. Yin, L. Cui, Z. Chen, The prevention effect of poly (L-glutamic acid)/chitosan on spinal epidural fibrosis and peridural adhesion in the post-laminectomy rabbit model. *Eur. Spine J.* **23**, 2423–2431 (2014).
47. M. Zeinalizadeh, S. M. Miri, F. A. Ardalan, F. Maleki, M. Zakeri, E. Aghajanzadeh, Z. Habibi, Reduction of epidural fibrosis and dural adhesions after lamina reconstruction by absorbable cement: An experimental study. *Spine J.* **14**, 113–118 (2014).
48. Y. He, M. Revel, B. Loty, A quantitative model of post-laminectomy scar formation. Effects of a nonsteroidal anti-inflammatory drug. *Spine (Phila Pa 1976)* **20**, 557–563 (1995).

Acknowledgments

Funding: This work was supported by the National Key Research and development program (2016YFC1101505), the National Natural Science Foundation of China (51873107, 81772312, and 81972078), Shanghai Jinshan District Science and Technology Committee, Medical and Health Science and Technology Innovation Fund project (2019-3-35), Shanghai Public Health Clinical Center, Fudan University, the Academy Project (KY-GW-2019-06), Shanghai Municipal Education Commission—Gaofeng Clinical Medicine Grant Support (20171906), and Science and Technology Commission of Shanghai Municipality (19440760400 and 18ZR1434200). **Author contributions:** Y.X., G.S., and J.T. prepared materials, designed and performed research, analyzed the data, and wrote the manuscript. R.C. prepared the materials and analyzed the data. X.S. and Y.G. performed the research in vitro. L.W., K.X., and Y.Z. performed the research in vivo. W.C. conceptualized and designed the research and outlined and edited the manuscript. L.C. designed the research and provided the laboratory space and funding. **Competing interests:** The authors declare that they have no competing interests. **Data and materials availability:** All data needed to evaluate the conclusions in the paper are present in the paper and/or the Supplementary Materials. Additional data related to this paper may be requested from the authors.

Submitted 11 April 2020
Accepted 25 September 2020
Published 25 November 2020
10.1126/sciadv.abc2036

Citation: Y. Xu, G. Shi, J. Tang, R. Cheng, X. Shen, Y. Gu, L. Wu, K. Xi, Y. Zhao, W. Cui, L. Chen, ECM-inspired micro/nanofibers for modulating cell function and tissue generation. *Sci. Adv.* **6**, eabc2036 (2020).